

Copyright Warning & Restrictions

The copyright law of the United States (Title 17, United States Code) governs the making of photocopies or other reproductions of copyrighted material.

Under certain conditions specified in the law, libraries and archives are authorized to furnish a photocopy or other reproduction. One of these specified conditions is that the photocopy or reproduction is not to be “used for any purpose other than private study, scholarship, or research.” If a user makes a request for, or later uses, a photocopy or reproduction for purposes in excess of “fair use” that user may be liable for copyright infringement,

This institution reserves the right to refuse to accept a copying order if, in its judgment, fulfillment of the order would involve violation of copyright law.

Please Note: The author retains the copyright while the New Jersey Institute of Technology reserves the right to distribute this thesis or dissertation

Printing note: If you do not wish to print this page, then select “Pages from: first page # to: last page #” on the print dialog screen

The Van Houten library has removed some of the personal information and all signatures from the approval page and biographical sketches of theses and dissertations in order to protect the identity of NJIT graduates and faculty.

ABSTRACT

ARTIFICIAL DIELECTRIC MATERIALS: SYNTHESIS AND OPTICAL CHARACTERIZATION OF SMALL METAL CLUSTERS EMBEDDED IN POLYMERIC MATRIX

by
Nazneen K. Shilpee

This study is concerned with the fabrication of films made of gold, nickel, and silicon clusters dispersed in a polymeric matrix. The films were fabricated by use of metal or semiconductor sputtering and plasma polymerization of Methyl Methacrylate monomer in a capacitively coupled RF (13.56 MHz) sputtering system. Optical transmittance and optical reflectance were measured as a function of wavelength. The optical absorption of metal or silicon clusters was studied as a function of cluster size. Cluster size and content were determined from Transmission Electron Micrographs (TEM). The absorption band resulting from a plasma resonance in the clusters was found to be shifted to the longer wavelengths as the metal cluster size and volume fraction increased. For gold, a linear relationship was obtained between the wavelength of the absorption peak and the deposition time, while, for nickel it was nonlinear. Overall, the clusters seemed to maintain their bulk properties in addition to size related plasma resonances.

**ARTIFICIAL DIELECTRIC MATERIALS:
SYNTHESIS AND OPTICAL CHARACTERIZATION OF
SMALL METAL CLUSTERS EMBEDDED IN POLYMERIC MATRIX**

**by
Nazneen Karim Shilpee**

**A Thesis
Submitted to the Faculty of the
New Jersey Institute of Technology
in Partial Fulfillment of the Requirements for the Degree of
Master of Science in Engineering Science**

Engineering Science Program

October 1994

Blank Page

APPROVAL PAGE

ARTIFICIAL DIELECTRIC MATERIALS:
SYNTHESIS AND OPTICAL CHARACTERIZATION OF
SMALL METAL CLUSTERS EMBEDDED IN POLYMERIC MATRIX

Nazneen Karim Shilpee

Dr. Haim Grebel, Thesis Advisor
Associate Professor of Electrical Engineering
of the Department of Electrical and Computer Engineering, NJIT

Aug 12, 94
Date

Dr. Roland A. Levy, Committee Member
Director of Materials Science and Engineering Program
and Professor of the Department of Physics, NJIT

8/14/94
Date

Dr. David Kristol, Committee Member
Director of Engineering Science
and Professor of the Department of Biomedical Engineering, NJIT

8/11/94
Date

BIOGRAPHICAL SKETCH

Author: Nazneen Karim Shilpee

Degree: Master of Science

Date: October 1994

Date of Birth:

Place of Birth:

Undergraduate and Graduate Education:

- Master of Science in Engineering Science,
New Jersey Institute of Technology,
Newark, NJ, 1994
- Master of Science in Physics,
University of Dhaka, Bangladesh, 1990
- Bachelor of Science in Physics,
University of Dhaka, Bangladesh, 1989

Major: Engineering Science

This thesis is dedicated to
my parents

ACKNOWLEDGMENT

The author wishes to express her sincere gratitude to her advisor, Professor H. Grebel, for his guidance, friendship, and moral support throughout this project. It was an honor to work under the guidance of such an esteemed researcher.

Special thanks to professors R. A. Levy and D. Kristol for serving as members of committee and providing valuable suggestions in this study.

The author is highly grateful to Dr. Yan Opyrchal for his timely help and suggestions. The author wishes to thank Stevens Institute of Technology for providing assistance to measure the film structure by TEM.

And finally, a sincere thank you to the author's family, especially, her husband, Ekramul Hasan Khan for his help and encouragement.

TABLE OF CONTENTS

Chapter	Page
1 INTRODUCTION	1
2 LITERATURE SURVEY	4
3 THEORY	8
3.1 Maxwell-Garnet Equation	9
3.2 Size Distribution	10
3.3 Mean Eccentricities	11
3.4 Three-dimensional Island Shapes	11
3.5 Average Interisland Distances	12
3.6 Effect of Grain Size on the Dielectric Constant	12
4 DIFFERENT METHODS OF THIN FILM DEPOSITION	14
4.1 Chemical Vapor Deposition	14
4.2 Physical Vapor Deposition	15
4.2.1 Vacuum Evaporation	15
4.2.2 Sputtering	16
5 MECHANISM OF FILM FORMATION	18
5.1 Formation Stages of Thin Films	18
5.2 Theoretical Studies of Cluster Formation Process	19
5.2.1 Kinetics	19
5.2.2 Clusters on Surfaces	20
5.3 Sputtering Kinetics and Film Growth	21
6 PLASMA POLYMERIZATION	24
6.1 Mechanistic Aspects of Plasma Polymerization	25
6.2 Parameters Involved In Plasma Polymerization	28

TABLE OF CONTENTS
(Continued)

Chapter	Page
6.3 Structure and Properties of Plasma Polymer Films	29
7 EXPERIMENTS	30
7.1 Polymer Film Fabrication Method	30
7.1.1 Experimental Setup for Plasma Polymerization	30
7.1.2 Substrate Preparation	30
7.1.3 Monomer Preparation	31
7.1.4 Polymer Deposition Procedure	31
7.1.5 Thickness Measurement	33
7.2 Metal Cluster Fabrication Method	34
7.2.1 Experimental Procedure	34
7.2.2 Transmission Electron Microscopy (TEM)	36
7.2.3 Determination of Metal Volume Fraction x	36
7.3 Optical Measurement System	37
7.3.1 Experimental Setup	37
7.3.2 Computer Program for Data Collection	38
7.3.3 Transmittance and Reflectance Measurement	38
8 EXPERIMENTAL RESULTS	39
8.1 Characterization of the Metal-Free Polymer Films	39
8.1.1 Deposition Rates	39
8.1.2 Refractive Index	39
8.1.3 UV-Visible Spectra	40
8.2 Structural Analysis of the Metallic Phase by TEM and Electron Diffraction ..	40

TABLE OF CONTENTS
(Continued)

Chapter	Page
8.2.1 Gold-Containing Samples	40
8.2.2 Nickel-Containing Samples	42
8.2.3 Silicon-Containing Samples	43
8.3 Analysis of Optical Transmittance Spectra	44
8.3.1 Gold Films	44
8.3.2 Nickel Films	47
8.3.3 Silicon Films	47
8.4 Analysis of Transmittance and Reflectance Spectra at 45° Incidence	51
9 DISCUSSIONS	53
10 CONCLUSIONS	58
APPENDIX A FIGURES SHOWING EXPERIMENTAL RESULTS	59
APPENDIX B COMPUTER PROGRAM FOR DATA COLLECTION	68
BIBLIOGRAPHY	78

LIST OF TABLES

Table		Page
7.1	Condition used for depositing Plasma Polymerized films of MMA	33
7.2	Summary of process parameters for metal cluster deposition	35
8.1	Properties of island films of gold	43
8.2	Properties of Nickel Islands	44

LIST OF FIGURES

Figure	Page
5.1 Schematic of different stages of film growth	19
5.2 Schematic diagram of a DC sputtering system	22
6.1 Schematic diagram of step-growth mechanism of plasma polymerization	26
6.2 Overall scheme of polymerization in glow discharge	27
7.1 Schematic diagram of RF sputtering system	32
7.2 Optical measurement system	37
8.1 TEM micrographs of 15 sec deposited gold particles [$x = 0.05$]	41
8.2 TEM micrographs of 30 sec deposited gold particles [$x = 0.10$]	42
8.3 Distribution of the number of gold particles as a function of gold cluster diameter from the TEM picture of Fig. 8.1	43
8.4 TEM micrographs of 7 min deposited nickel particles [$x = 0.13$]	45
8.5 Normal transmittance of successive gold/polymer layers. Deposition time: Gold-30 sec, Polymer-5 min. Top curve- 1st layer, Lowest curve- 6th layer	46
8.6 Normal transmittance of successive gold/polymer layers. Deposition time: Gold-30 sec, Polymer-2 min. Top curve- 1st layer, Lowest curve- 6th layer	46
8.7 Normal transmittance of successive gold/polymer layers. Deposition time: Gold-1 min, Polymer-5 min. Top curve- 1st layer, Lowest curve- 6th layer	48
8.8 Normal transmittance of successive gold/polymer layers. Deposition time: Gold-1 min, Polymer-2 min. Top curve- 1st layer, Lowest curve- 6th layer	48
8.9 Variations of absorption peak with deposition time for various gold films	49

LIST OF FIGURES
(Continued)

Figure	Page
8.10 Normal Transmittance curves of gold samples for different deposition time. The deposition time of each film is given in Table 8.1	49
8.11 Normal transmittance curves of one layer of nickel for different deposition time. Deposition time of each layer is given in Table 8.2	50
8.12 Variations of absorption peak with deposition time for various nickels films	50
8.13 Transmittance and reflectance curves of 6 layers of gold at 45° incidence. Deposition time: Gold- 15 sec, Polymer- 2 min. Curve (1): Transmission (2): Reflection	51
8.14 Transmittance and reflectance curves of 6 layers of nickel at 45° incidence. Deposition time: Nickel- 10 min, Polymer- 2 min. Curve (1): Transmission (2): Reflection	52
8.15 Transmittance and reflectance curves of 3 layers of silicon at 45° incidence. Deposition time: Silicon- 6 min, Polymer- 5 min. Curve (1): Transmission (2): Reflection	52
A.1 Normal transmittance of successive nickel/polymer layers. Deposition time: nickel-10 min, Polymer-2 min. Top curve- 1st layer, Lowest curve- 6th layer	60
A.2 Normal transmittance of three layers of nickel each 12 min separated by 5 min polymer	60
A.3 TEM micrographs of 45 sec deposited gold particles [$x = 0.15$]	61
A.4 Electron diffraction pattern of 45 sec deposited gold. Closed bright circles represent crystallinity	62
A.5 Comparison of computed and measured optical transmittance (circles and solid curves) for discontinuous gold films with five mass thicknesses [3]	63

**LIST OF FIGURES
(Continued)**

Figure	Page
A.6	Normal transmittance of six layers of gold for two different samples. (1) Deposition time: gold- 30 sec;; polymer- 2 min. (2) gold- 1 min; polymer- 5 min 63
A.7	TEM micrographs of 9 min deposited nickel particles [$x = 0.17$] 64
A.8	Electron diffraction pattern of 9 min deposited nickel. Closed bright circles represent crystallinity 65
A.9	Normal transmittance of 10 min plasma polymerized methyl methacrylate 66
A.10	Normal transmittance of one layer of silicon. (1) 30 min deposition by RF sputtering. (2) 30 min deposition by magnetron sputtering 66
A.11	Normal transmittance of successive silicon/polymer layers. (1) 3 layers of silicon, (2) 6 layers of silicon. Deposition time: silicon- 12 min; polymer- 5 min 67
A.12	Normal transmittance of successive silicon/polymer layers. (1) 3 layers of Si. Deposition time: Si- 12 min; polymer- 5 min (2) 4 layers of Si. Deposition time: Si- 6 min; polymer- 5 min. (3) 3 layers of Si. Deposition time: Si- 6 min; polymer- 5 min 67

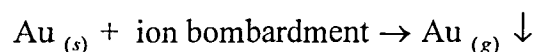
CHAPTER 1

INTRODUCTION

During the past few years there have appeared a large number of works investigating the optical properties of discontinuous thin films of Au, Ag, and Cu [1-3]. Technological applications for these thin films have been of interest recently since they offer flexibility of synthesis and have the potential for fabricating novel dielectric materials [4]. Usually, a two-component effective medium theory has been applied to interpret much of the reported data [5]. Dispersion of metallic particles in a polymeric matrix is interesting from several points of view. Basic studies such as the investigation of optical or electrical properties can be performed on these composite systems as a function of the metal dispersion [6]. Applications of these materials in the field of optical filters, magnetic, or optical recording, have been postulated. These materials are very useful in fabricating graded index passive or active devices such as optical waveguides, optically controlled microwave transmission lines, lenses, etc., for integrated optical and microwave circuits.

Small semiconductor clusters dispersed in polymeric matrix represent a new class of material. Extensive studies on the nonlinear optical properties of semiconductor clusters confined in polymers, have demonstrated interesting new physics and novel device applications. Different techniques are available for the preparation of these films, e.g., plasma polymerization of organometallic molecules, metal evaporation and plasma polymerization, co-sputtering of metal and polymer, reactive ion etching, and plasma polymerization in a capacitively rf discharge. This latter technique, extensively explored by Kay, Dilks, and Hetzler [7], relies on the concept of physical sputtering of a metal target by ion bombardment from a rare-gas plasma. When sufficient fluorocarbon monomer is injected into such a plasma, deposition will take place at all grounded surfaces, whereas on the rf-powered electrode, metal removal by ion bombardment

enhanced chemical etching together with physical sputtering, will dominate. The degree to which this process dominates over the polymerization deposition process depends on the ratio of etchant to polymerization species arriving at a particular surface as well as the kinetic energy of the incident ions [6]. In the case of a chemically inert metal, e.g., gold, no chemical reactions are expected between the metal and the reactive species of the discharge. So gold can only be removed from the powered electrode by physical momentum transfer sputtering according to the following process [8]:



This chemical simplicity allows relatively straightforward interpretation of the plasma diagnostic schemes such as optical emission spectroscopy and mass spectrometry. When the metallic target consists of a reactive metal, such as cobalt, then reactions in a fluorocarbon plasma and at the surface of the growing film between fluorine atoms and the metal lead to the formation of metal fluoride particles, CoF and CoF₂, within an organic matrix [8]. With a reactive metal, therefore, there is a more complex system: polymeric, metallic, metal fluoride, and even metal oxide, if no diffusion barrier is deposited on the thin-film surface to prevent post-deposition oxidation.

In order to avoid such compositional complexity during plasma polymerization in the presence of a reactive metal, a hydrocarbon instead of a fluorocarbon can be injected into the plasma, thereby eliminating the very highly reactive fluorine atoms. In this approach the main problem is to prevent the formation of a permanent carbonaceous layer at the surface of the powered metallic target. Controlled metal incorporation into polymeric matrices is of considerable interest because the metal species can dramatically influence both the chemical and physical properties of the resultant polymer [9]. Alternately, the dielectric polymeric matrix can serve to isolate the metallic clusters from one another thereby facilitating the study of such clusters.

In this thesis we are reporting the synthesis of thin composite films (Artificial Dielectrics) containing metal and semiconductor clusters in plasma polymerized matrices.

These films were produced by successive layers of plasma polymers (from a hydrocarbon monomer) and metal clusters deposited by RF sputtering from a metal target. The composites were then analyzed by optical transmittance measurements and Transmission Electron Microscopy (TEM) techniques. Plasma polymers offer the advantage of producing a very thin, continuous layer. The encapsulation of the metal particles by an amorphous polymer matrix prevents the formation of a cohesive metal layer. Therefore, a cluster is also formed with higher metal content. Simultaneously, the embedding of the metal clusters in the polymer matrix provides for the necessary stability of the metal clusters, and maintains their properties stored in air.

The structure and consequently the optical properties of the composite thin film depend on the condensation of the metal cluster from the gas phase [10]. Clustering of the sputtered material is a naturally occurring processes at the nucleation sites on the substrate. The process leads to a three dimensional island formation in the initial stages of film growth. The three-dimensional island shapes are extremely important since they strongly influence not only the location of the transmittance minima but also the overall magnitude of the transmittance. When homogeneous film is desired, high substrate temperature is required to suppress the island growth.

This thesis contains 9 chapters. The previous fundamental studies on discontinuous thin films are discussed chronologically in Chapter 2. Theory is discussed in chapter 3. Various techniques for film deposition are described in Chapter 4. In chapter 5, kinetics of cluster formation is described. In Chapter 6, plasma polymerization process is explained theoretically. The film preparation and experimental characterizations are analyzed in Chapter 7. The results of this study are summarized in Chapter 8. Discussions of experimental results are in Chapter 9. Finally conclusions and recommendations are made in Chapter 10.

CHAPTER 2

LITERATURE SURVEY

There are a number of publications concerned with metal cluster in polymer matrix. In recent years, plasma polymerization of metal and semiconductor containing organic films have been gaining special attention owing to their interesting electrical, optical, and chemical properties. In this chapter a review of research on metal cluster in polymeric matrices is presented.

During the last decade the physical properties of gold containing plasma polymerized fluorocarbon (Au/PPFC) films have been studied by Kay *et al* [11-13] and by others [14,15, 30]. Perrin and co-workers [13] investigated the optical properties of similar films over a wide range of gold volume fractions and correlated the optical properties with the microstructure of the films. Those studies revealed that the microstructure and cluster size distribution and concomitantly the physical properties of Au/PPFC can be changed by postdeposition annealing.

The electrical properties of gold containing PPFC films have been investigated by Perrin *et al.* [11] and by Laurent and co-workers [12]. They observed that the films are very good insulators at low gold volume fraction p ($p < 0.2$) and are good conductors at high volume fraction ($p > 0.6$). The electrical percolation threshold was found at $p_c = 0.37 \pm 0.03$. In a narrow range of p around this threshold the electrical properties of the films change from an insulator to a conductor, accompanied by a drop of the electrical resistivity from about $10^{12} \Omega \text{ cm}$ at $p = 0.3$ to about $10^{-4} \Omega \text{ cm}$ at $p = 0.5$.

Parmigiani *et al.* [5] studied the optical properties of gold particles, sputtered at different substrate temperatures. The gold particles sputtered on glass substrate were analyzed by both optical absorption and transmission electron microscopy techniques. The sputtering system was a Balzers Sputron II, modified in order to control the time of

sputtering from 1 to 30 sec. The substrate temperature could be changed from 25 to 250° C. From the films deposited at 160° C, shifting of the absorption maxima to the red, due to the increase of the filling factor, was seen, as was predicted by Maxwell-Garnet (M-G) theory. The anomalous absorption peak of the "cold" films shifts smoothly toward lower energies with increasing f , whereas the peak of the "hot" films depend much on the volume fraction. Finally they concluded that the characteristic parameters of the anomalous absorption band of thin discontinuous films are related to the growth process, i.e., different growth conditions cause a change of the energy position, width, and intensity of the plasma absorption. These facts suggests that the optical constants of the metallic clusters are different from those of the bulk and dependent on the growing conditions.

Laser coalescence of gold clusters in gold-fluorocarbon composite films was presented by Paul *et al.* [16]. In their work, it was demonstrated that bulk heating or annealing of an rf plasma deposited gold/fluorocarbon leads to film collapse from a metastable polymer state, with concomitant microstructural changes in the size and shape of the gold clusters. A focused, visible laser beam was used to coalesce the gold clusters within the PPFC matrix. Heating the composite with the laser causes the film to collapse with a loss of weight due to decomposition and volatilization of the polymer. Under the appropriate laser power and scanning conditions, coalescence of the gold particles results in a conducting metal line, exhibiting close to bulk metal resistivity.

The ability to produce transition-metal clusters dispersed in a polymeric matrix was investigated by Laurent *et al.* [6]. They found that it was possible to obtain transition-metal clusters, e.g., cobalt clusters, dispersed in a plasma-polymerized hydrocarbon matrix by making appropriate changes in the experimental plasma conditions whereas in a fluorocarbon matrix, formation of metal fluoride can not be avoided due to the high chemical reactivity of F atoms in the plasma. In the case of chemically inert metal, e.g., gold, no chemical reactions were expected between the metal

and the reactive species of the discharge. Films containing from 0% up to 100% of metal can be produced simply by monitoring the inert gas to hydrocarbon monomer partial pressure ratio mass spectrometrically. The shape and size of gold and cobalt particles at equivalent volume fractions were shown to be different, which was reflected in different electrical percolation threshold values for the two systems.

The optical properties of aggregated gold films have been studied by Truong *et al.* in the visible and near infrared [32]. Their analysis showed that it is possible to use a rotational-ellipsoid model to describe the optical properties of aggregated gold films. From transmittance spectra they observed two dips in the curves; one near 400 nm remains at that wavelength, which proves the existence of interband transition, whereas the other dip shifts from about 530 nm to 600 nm as the thickness increases due to the plasma resonance in the particles. They also found that variations of the resonance wavelength with the film thickness is nonlinear.

C. Laurent *et al.* [12] have reported the dielectric breakdown behavior of gold-containing plasma-polymerized polytetrafluoroethylene thin films prepared in an rf glow discharge. The films showed a wide range of conductivities from insulating ($\rho > 10^{16} \Omega\text{cm}$) to metallic ($\rho \sim 3 \times 10^{-6} \Omega\text{cm}$), depending on plasma conditions during synthesis. The analysis of current-voltage characteristics in the dielectric regime showed that the conduction was volume limited in pure plasma-polymerized thin films (Poole-Frenkel type of conduction). A bistable switching behavior was observed in samples containing more than 10% gold. Dielectric breakdown measurements were realized on self-healing metal-insulator-metal structures. They noticed that the breakdown strength decreased from 1.8 to 0.8 MV/cm when the gold concentration increased from 0% up to 10%. After this initial change, the evolution was smooth until very near percolation (0.55 MV/cm for 34.5% of gold). The leaking current became important ($\sim 10^{-3} \text{ A/cm}^2$) at high field, which demonstrated that there exists a great number of tunneling paths over the whole composite structures.

Model systems of evaporated gold particles on polystyrene (PS) and poly (2-vinylpyridine) (PVP) were described by Martin *et al.* [17]. It was found that the fluid character of the polymer substrates at the annealing temperature of interest allows one to control the coalescence rate, thereby providing a unique method for controlling the microstructure of discontinuous metal films. Cross-sectional transmission electron microscopy showed that the coalescence rate for gold particles in a PVP matrix was much less than the coalescence rate for gold particles in a PS matrix, indicating that polymer/metal interactions play an important role in the determination of the coalescence rate.

Optical plasma-resonance absorption of small Ni particles have been measured by Anno *et al.* [33] in the photon energy region of 1.5 eV to 6.5 eV. A strong localizing tendency has been found for conduction electrons of Ni by investigating the optical absorption of Ni island films and continuous Ni films. They explained this tendency by the enhanced correlation interaction between the conduction electrons in the dynamical state due to the incidence of light. They concluded the broad absorption in the region from 1.5 to about 3.5 eV is the optical plasma resonance absorption of Ni island films.

The UV-Visible spectra of Ni colloid were reported by Moskovits *et al.* [34]. They noticed the absorption spectrum of colloidal nickel ranging from 300 to 400 nm which arises from the plasma resonance of the particles. They also mentioned from another reference about the absorption of bulk nickel due to the interband transition which was at 230 nm.

CHAPTER 3

THEORY

The optical properties of discontinuous metallic films or granular composite films, consisting of metal clusters embedded in a dielectric, have been of interest since the beginning of the century when Maxwell-Garnett (MG) described the first theoretical framework to explain the resonant absorption or dielectric anomaly which characterizes such systems [13]. The clusters in the discontinuous films are orders of magnitude smaller than the wavelength of the incident light. Hence the optical properties of the deposits can be characterized in terms of an effective medium theory (e.g., M-G type theory), being a spatial average over the dielectric permeabilities for the metal islands and for their surrounding medium. This theory holds in the case of gold for clusters with sizes of the order of 10 nm or less. In this theory, the dielectric function of the composite medium is related to the polarizability of a single metallic particle surrounded by the dielectric via the Clausius-Mossotti (CM) equation. There have been numerous investigations on Cu, Ag, and Au discontinuous films [3], Au or Ag colloidal particles, or cermet films, such as Ag-SiO₂ or Au-SiO₂ to verify the applicability of the MG theory. Although this theory correctly predicts the position of the anomalous absorption peak in the visible region at low metal volume fraction and for small spherical particles, it fails to describe the evolution of the optical absorption spectrum at high metal volume fraction when the metal clusters are interconnected and no longer spherical. This limitation comes essentially from the fact the MG theory does not treat the metal and the dielectric phase on a symmetrical basis as a function of volume fractional changes. In spite of these intrinsic limitations, the MG theory has been refined to take into account the effect of particle shape in the form of ellipsoids, the effect of multiple interactions between spherical particles, and more recently the effect of topological disorder.

As is well known, island films consisting of many small metal particles show the anomalous optical absorption, which results from the plasma resonance absorption. The incident light polarizes the conduction electron gas of the metal particle, producing an electric moment which oscillates with the frequency of the light ω [31]. When ω approaches the natural frequency of the electron gas in the particle, a resonant absorption occurs. The absorption of particles smaller than about 20 nm in diameter is caused mainly by the electric dipole oscillation.

3.1 Maxwell-Garnet Equation

The basic MG equation applies to small spherical metal particles assuming that the wavelength of light is much greater than the size of the particles. For normal incidence (electric vector of the light parallel to the plane of the film) the relative dielectric constant ε of a collection of particles is given by [37]

$$\varepsilon = 1 + 12\pi N\alpha / (3 - 4\pi N\alpha) \quad (3.1)$$

where N is the number of metallic particles per unit volume, α is the polarizability of an individual particle. The polarizability of a metallic particle of radius r embedded in a dielectric medium of dielectric constant ε_d can be written as

$$\alpha = r^3(\varepsilon_m - \varepsilon_d) / (\varepsilon_m + 2\varepsilon_d) \quad (3.2)$$

where ε_m is the dielectric constant of the metal. Substituting Eq. (3.2) into Eq. (3.1) an effective dielectric constant ε is obtained as follows

$$\frac{\varepsilon - \varepsilon_d}{\varepsilon + 2\varepsilon_d} = f \left(\frac{\varepsilon_m - \varepsilon_d}{\varepsilon_m + 2\varepsilon_d} \right) \quad (3.3)$$

where $f = 4\pi N r^3 / 3$ is the volume fraction occupied by the particles. From Eq. (3.2) and (3.3) it can be deduced that the polarizability of each individual cluster affects the characteristics of the dielectric medium as a whole.

To understand the theoretical explanation of the optical transmittance the following parameters should be discussed [3].

3.2. Size Distributions

It is clear from the electron micrographs in Fig. 8.1 that the metal islands exhibit a size distribution. Its shape depends on the coarsening mechanism, which is coalescence dominated. Coalescence can be treated as a series of binary events, where in each step two islands merge to form one larger island. For coalescence growth a statistical model [3] can be used which predicts that the logarithm of the island volumes should have a Gaussian distribution. In the case of spherical particles the fractional number of particles Δn per logarithmic diameter interval $\Delta(\ln d)$, can be written as

$$\Delta n = f_{LN}(d) \Delta(\ln d) \quad (3.4)$$

where,

$$f_{LN}(d) = \frac{1}{(2\pi)^{1/2} \ln(\sigma_d)} \exp\left[-\frac{1}{2} \left(\frac{\ln(d/\bar{d})}{\ln \sigma_d}\right)^2\right] \quad (3.5)$$

which defines a *log-normal distribution function* (LNDF). In Eq. (3.5), \bar{d} is the mean of the sphere diameters and σ_d is the geometric standard deviation of the diameters. Eqs. (3.4) and (3.5) provide a means by which the coalescence process can be quantified. Empirically, the LNDF has been shown to constitute an excellent approximation for experimental size distributions of islands in discontinuous noble metal films, inert gas evaporated particles, supported metal catalysts, and some colloidal particles.

The electron micrographs show that the metal islands look far from circular, in particular for the larger thicknesses. A reasonable approximation for the projected area of a film particle is to describe it as being an ellipse with an area $(\pi/4)ab$, where a is the major axis and b is the minor axis. Evaluation of a and b for discontinuous gold films on

glass substrates were analyzed by Andersson and Granqvist [3], where the data were also compared with LNDF's.

3.3. Mean Eccentricities

A quantification of the average deviation from circularity for the islands in the discontinuous films is convenient for a description of their optical properties. As a starting point the eccentricity e of an ellipse is by definition

$$e^2 = 1 - (b/a)^2 \quad (3.6)$$

The optical properties are not directly related to the e 's and therefore no unique mean eccentricity can be given for an ensemble of islands. However, an obvious definition can be written as

$$\bar{e}_0^{-2} = 1 - (\bar{b}/\bar{a})^2 \quad (3.7)$$

Another definition is

$$\bar{e}^{-2} = 1 - \left(N^{-1} \sum_{k=1}^N \frac{a_k}{b_k} \right)^{-2} \quad (3.8)$$

which puts most weight on the islands with largest elongation. Neglecting the conditions $a_k \geq b_k$, which is of course a rather gross simplification, one can show that

$$\bar{e}^{-2} \approx 1 - (\bar{b}/\bar{a})^2 \exp(-4 \ln^2 \sigma) \quad (3.9)$$

Usually mean eccentricity is gradually enhanced when the average film thickness is increased.

3.4. Three-dimensional Island Shapes

To this point we have been discussing only the two-dimensional images of the islands, as seen in the electron micrographs, whereas the optical properties are governed by their three-dimensional structure. For the case of film particles represented by whole prolate spheroids (formally obtained by rotating an ellipse around its major axis) a relation

$$t - q = \frac{2}{3} A \bar{x} (1 - \bar{e}^2)^{1/4} \exp(3/2 \ln^2 \sigma) \quad (3.10)$$

should be approximately fulfilled. In Eq. (3.10) $t-q$ denotes an effective film thickness, which takes into account the fact that the amount of material impinging towards the substrate is not necessarily equal to the amount located on its surface as visible islands. This lost thickness is called q . If t vs the expression in the right side of Eq. (3.10) is plotted a linear relationship is obtained for small t , indicating that a model of whole prolate spheroids is a good approximation for the three-dimensional shape of the islands at $t \leq 3$ nm. At larger thicknesses the points fall well above the line. The most reasonable explanation is that the spheroidal approximation breaks down.

3.5. Average Interisland Distances

Not only are the island sizes and shapes important for understanding the optical properties but also the average interisland separation is needed. One obvious experimental way to determine this quantity is to select an arbitrary area containing 100 islands, and measure for each of these the smallest center-to-center distance to its neighbors, D_{\min} . The average interisland separation can be written as

$$D \approx \xi(p) \bar{x} / A^{1/2} \quad (3.11)$$

for islands of equal diameter \bar{x} placed on a regular two-dimensional lattice such that an area fraction A is covered with islands. The prefactor $\xi(p)$ depends on the coordination number p of the lattice.

3.6. Effect of Grain Size on the Dielectric Constant

The relative dielectric constant of a metal $\epsilon_m(\lambda)$, in the presence of optical beam is decomposed into a free-electron part $\epsilon_m^{(f)}(\lambda)$ and an interband part $\epsilon_m^{(i)}(\lambda)$ [13],

$$\epsilon_m(\lambda) = \epsilon_m^{(f)}(\lambda) + \epsilon_m^{(i)}(\lambda) \quad (3.12)$$

where,

$$\varepsilon_m^{(f)}(\lambda) = 1 - \frac{\lambda^2}{\lambda_0^2} \frac{1}{(1 + i\lambda / 2\pi c\tau)} \quad (3.13)$$

according to the Drude theory. Here, λ_0 is the plasma wavelength (133 nm for gold), and τ the mean free electron relaxation time which is effected by the grain size x . Neglecting quantum-size effects, which are expected to be hardly detectable by optical absorption measurements, a classical treatment of the electron scattering in a grain gives

$$\tau^{-1} = \tau_b^{-1} + 2v_F / x \quad (3.14)$$

where τ_b is the bulk-metal mean free-electron relaxation time corresponding to a mean free path of 380 Å for bulk gold, and v_F is the Fermi velocity (1.39×10^8 cm/sec for gold). At optical wavelengths, $(\lambda / 2\pi c\tau)^2 \ll 1$, so the following approximation can be used:

$$\varepsilon_m^{(f)}(\lambda) = 1 - \frac{\lambda^2}{\lambda_0^2} + i \frac{\lambda^3}{\lambda_0^2} \frac{1}{2\pi c\tau} \quad (3.15)$$

assuming that the interband part is not affected by the grain or cluster size, $\varepsilon_m(\lambda)$ can be written as

$$\varepsilon_m(\lambda) = \varepsilon_{bm}(\lambda) + i \frac{\lambda^3}{\lambda_0^2} \frac{v_F}{\pi c x} \quad (3.16)$$

where $\varepsilon_{bm}(\lambda)$ is the relative bulk dielectric constant.

CHAPTER 4

DIFFERENT METHODS OF THIN FILM DEPOSITION

Thin film fabrication is a complicated process which involves control of many processing parameters. The time of processing, equipment cost, throughput and quality of films are important factors for a successful commercial production. Many techniques are available in the present technology for film fabrication. Most common methods used for economical production are physical vapor deposition (PVD) and chemical vapor deposition (CVD). This chapter describes these two methods in brief.

4.1 Chemical Vapor Deposition

Chemical vapor deposition is defined as the formation of a non-volatile solid film on a substrate by the reaction of vapor phase chemicals (reactants) that contain the required constituents. The reactant gases are introduced into a reaction chamber and are decomposed and reacted at a heated surface to form the thin film. CVD is a widely used method in semiconductor technology for the preparation of thin monocrystalline films of high purity [18]. CVD process has several advantages over other methods of film deposition which make it one of the popular methods adapted commercially. These are:

- i) conformal step coverage can be achieved by this method.
- ii) stoichiometric control of the film can be easily achieved by adjusting the processing parameters such as deposition temperature, flow rate etc.
- iii) high throughput is possible.
- iv) low maintenance cost makes it an attractive method for large scale production.

However, CVD has the following limitations:

- i) The design of the reactor to obtain a uniform deposition is the most critical part.

- ii) The use of many unwanted and possibly deleterious toxic, explosive or corrosive gaseous reactants which must be eliminated.
- iii) The use of very high temperature.

4.2 Physical Vapor Deposition

In this method thin film material in gaseous form is allowed to deposit on the substrate directly. No chemical reaction is involved in this method. The most important physical methods for the preparation of thin film are cathode sputtering and vacuum evaporation. Both methods require low pressure in the working space and therefore make use of vacuum techniques.

4.2.1 Vacuum Evaporation

Vacuum evaporation is currently the most widely used method for the preparation of thin films. The method is comparatively simple, though it may provide films of extreme purity and, to a certain extent, of preselected structure in proper experimental conditions. The process of film formation by evaporation consists of several physical stages [18]:

- i) transformation of the material to be deposited by evaporation or sublimation into the gaseous state.
- ii) transfer of atoms (molecules) from the evaporation source to the substrate.
- iii) deposition of these particles on the substrate.
- iv) the rearrangement or modifications of their binding on the surface of the substrate.

Evaporation has been widely utilized for depositing Al and other metallic films in microelectronics fabrication. Some of the characteristics that are responsible for the widespread use of evaporation include [19]:

- i) films can be deposited at high rates (e.g. 0.5 $\mu\text{m}/\text{min}$ for Al).
- ii) no substrate surface damage as the energy of the impinging atom is low (~ 0.1 eV).

iii) high purity films can be achieved due to high vacuums under which evaporation is performed. However, evaporation suffers from the following limitations:

i) accurately controlled alloy compositions are more difficult to achieve with evaporation than with sputtering.

ii) *in situ* cleaning of the substrate surfaces is not possible with evaporation systems.

iii) x-ray damage, caused by electron-beam evaporation processes, is avoided in sputter deposition.

4.2.2 Sputtering

Sputtering is vaporization of a material by bombarding it with high-energy atoms and ions of argon or other inert gases. The force of impact causes atoms or molecules to be ejected from the surface by momentum transfer. These ejected atoms, which can be charged and in some cases molecular species, deposit at the substrate. Sputtering has become the most widely utilized deposition technique for a variety of metallic films in VLSI fabrication, including aluminum, aluminum alloys, platinum, gold, titanium:tungsten and tungsten. Sputtering has displaced evaporation as the workhorse PVD method for thin film deposition because of the following advantages [19]:

i) Sputtering can be accomplished from large-area targets, which simplifies the problem of depositing films with uniform thickness over large wafers.

ii) Film thickness control is easily achieved by selecting a constant set of operating conditions and then adjusting the deposition time to reach it.

iii) Many important film properties, such as step coverage and grain structure, can be controlled by varying the negative bias and heat applied to the substrates.

iv) The surface of the substrates can be sputter-cleaned in vacuum prior to initiating film deposition.

v) Device damage from x-rays generated during electron beam evaporation is eliminated.

As is true with other processes, however, sputtering also has its drawbacks. They are:

- i) high equipment cost
- ii) low deposition rates for some materials (e.g. SiO_2).
- iii) impurity incorporation in the film due to deposition in low-medium vacuum conditions.

The common methods of thin film deposition, namely PVD and CVD, were described. Their advantages and disadvantages were mentioned. Sputtering was found to be suitable method for cluster fabrication. Therefore, in this experiment, sputtering technique has been used to prepare composite films of successive metal/polymer layers.

CHAPTER 5

MECHANISM OF FILM FORMATION

5.1 Formation Stages of Thin Films

Principally, three different mechanisms of thin film condensation can be distinguished, depending on the strength of interaction between the atoms of the growing film and between the atoms of the film and the substrate [18]: (i) the layer-by-layer growth (van der Merwe mechanism); (ii) a three-dimensional nucleation, forming, growth, and coalescence of islands (Volmer-Weber mechanism); (iii) adsorption of a monolayer and subsequent nucleation on top of this layer (Stranski-Krastanov mechanism). In most cases mechanism (ii) takes place. It has been found by observation of films evaporated directly in the viewing field of an electron microscope that film growth can usually be divided into certain stages. These are as follows:

(1) Nucleation, during which small nuclei are formed that are statistically distributed (with some exceptions) over the substrate surface.

(2) Growth of the nuclei and formation of larger islands, which often have the shape of small crystals (crystallites).

(3) Coalescence of the islands (crystallites) and formation of a more or less connected network containing empty channels.

The process is schematically shown in Fig. 5.1 [20]. From above description it is clear that film morphology changes with time i.e., with thickness and thickness depends on a number of parameters such as target material used, surface condensation, surface temperature, discharge power and deposition rate.

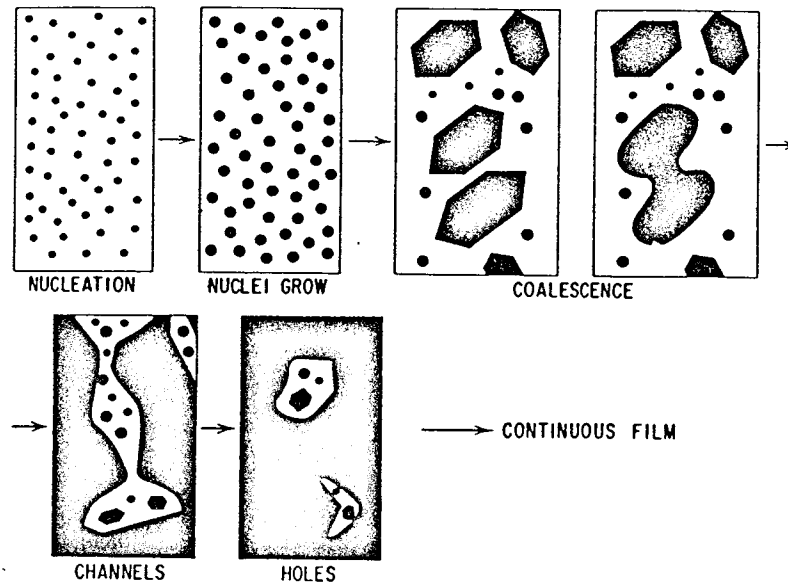


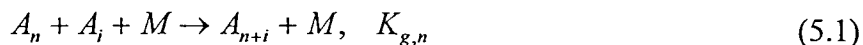
Figure 5.1 Schematic of different stages of film growth

5.2 Theoretical Studies of Cluster Formation Process

There are several approaches to the theory of cluster growth. A macroscopic kinetics approach for growth of clusters will be considered here.

5.2.1 Kinetics

The various detailed reaction mechanisms proposed to explain the kinetics of cluster and surface growth share several features in common which are outlined below [22-24]. The usual kinetics approach is to consider the following sort of mechanism:



Equation (5.1) represents the growth of a cluster of size n by aggregation of a cluster of size i . It is usually assumed that $i = 1$, i.e., the growth is by accretion of monomers. K_g and K_e are rate constants for growth and rate constants for evaporation. The involvement of a third body M is necessary to remove the energy of condensation, otherwise there is

always sufficient energy to evaporate an atom from the newly formed cluster. This is especially important for very small clusters. For large clusters, the third body nature of the growth terms can be ignored, where the growth is by means of binary processes and decay by means of unimolecular processes.

For many cluster sizes there may be a time delay between this energy removal collision and the formation collision because the excess energy of condensation is rapidly distributed among the internal modes of the cluster. Eq. (5.2) represents the spontaneous evaporation of monomers from the surface of a cluster. Energetics would indicate that monomers are the only particles that easily leave a homonuclear cluster. Various models [22-24] usually give rise to the notion of a critical-size cluster. Clusters below this critical size decay faster than they grow. A common result of most of these models is that the population of clusters decreases exponentially with number of atoms for free clusters. Most experimental studies of cluster-size distributions confirm these predictions.

5.2.2 Clusters on Surfaces

A film produced by deposition of atoms or particles on a surface forms in several stages: (1) nucleation, (2) cluster growth, (3) coalescence, (4) further thickening, and (5) recrystallization (perhaps) [23]. We will be concerned with steps (1) - (2).

Neidermayer [23] as well as Weeks and Gilmer [24] have modeled the kinetics of cluster growth. Nucleation occurs at specific sites, often associated with lattice defects on the substrate. Cluster growth commences as atoms impinge near each other; in a series of experiments it was found that gold atoms will be captured if they land within 6.5 \AA of a growing cluster. As cluster growth continues, the energetics regarding two-dimensional or three-dimensional growth must be considered. Calculations indicate that if the heat of vaporization of the metal (Λ_v) is greater than three times the heat of desorption of the metal atom from the surface (E_{des}), three-dimensional clusters should form. However, if the heat of metal vaporization is less than three times the energy of desorption minus the

energy of diffusion (E_{diff}), two-dimensional cluster growth is favored [23]. Depending on the surface, E_{des} and E_{diff} will vary as

$$\Lambda_o \geq 3E_{des} \quad (\text{three-dimensional favored}),$$

$$\Lambda_o \leq 3(E_{des} - E_{diff}) \quad (\text{two-dimensional favored}).$$

These theoretical considerations predict that metal clusters growing on most clean metal surfaces and semiconductors would grow initially in two dimensions, and this is found experimentally [23]. Neidermayer has treated cluster growth as a polymer growth problem. The growth process becomes governed by an equilibrium between impingement and desorption, which is indicated by a constant value of monomer concentration over a considerable time period. So at a certain substrate temperature it should be possible to establish equilibria with very small cluster sizes. However, at low substrate temperatures no such equilibria can be established, and cluster and nucleus concentrations rise very steeply. Generally, the cluster growth for gold under low-temperature conditions (80 K) on a clean surface involves an induction period of 10^{-5} s, twin formation until 10^{-3} s, constant growth to 10^{-1} s, and then coalescence to a film [23].

5.3 Sputtering Kinetics and Film Growth

Sputtering phenomena is characterized as a momentum transfer process in which argon or other ions and atoms from a plasma bombard a target material. The collision of the argon atoms and ions with the surface atoms and molecules of the target knocks off (sputters) the target material, which then forms a deposit on the substrate. Under a glow discharge plasma in the presence of an inert gas pressure, low energy ion-beams can be generated. It is believed that the surfaces of solid erode under ion bombardment and then the erosion rates are characterized primarily by the sputtering yield as:

$$S = \text{mean number of emitted atoms / incident particle} \quad (5.3)$$

The sputtering yield is important because it largely determines the rate of sputter deposition. Sputter yield depends on a number of factors besides the direction of incidence of the ions, including: i) target material; ii) mass of bombarding ions; iii) the energy of bombarding ions. There is a minimum energy threshold for sputtering that is approximately equal to the heat of sublimation (e.g. 13.5 eV for Si) [19]. In the energy range of sputtering (10-5000 eV), the yield increases with ion energy and mass.

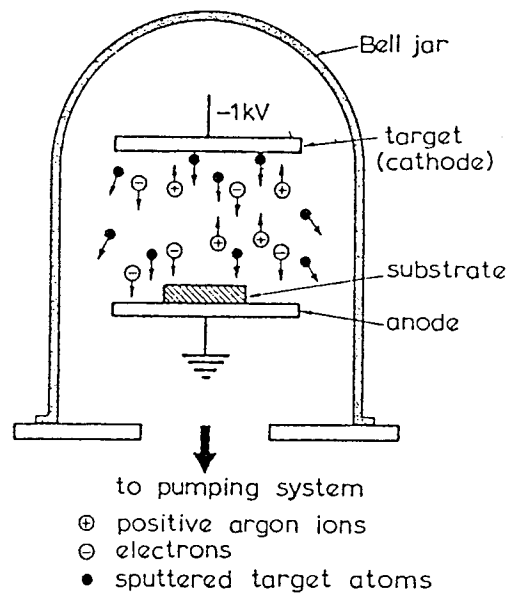


Figure 5.2 Schematic diagram of a DC sputtering system

Fig. 5.2 represents schematically a glow discharge sputtering system, where the target to be deposited is connected to a negative (DC or AC) voltage. The substrate holder, which is in general grounded and heated, faces the solid target. A gas is introduced in a chamber to produce sputtering ions, where gas pressure ranging from a few mTorr to about 100 mTorr are used and the most common sputtering gas is Ar. At fixed voltages, when the pressure is increased, the electron mean free path decreases and larger currents are possible to flow. At high pressures the transport of the sputtered atom

is reduced by collisional scattering, with typical sputtering conditions placed between 80 and 140 mTorr. The sputter-deposition rate is approximately given [21] as follows:

$$D = 62.3 \frac{SJM}{P} F \quad (5.4)$$

where J is the ion current, S is the sputtering yield, P is the density of target material, M is the average atomic weight and F takes a value between 0.1 and 0.5. From Eq. (5.4), it is apparent that the sticking speed of atoms is critically dependent upon the SJ product. So it can be concluded that since S is approximately proportional to an applied voltage V , D is a function of the VJ product which is defined as an important parameter of the sputtering apparatus. It had so far been obtained that the rates are linearly proportional to the input power and decreases with increasing a target-substrate distance.

When the glow discharged is initiated and maintained, positive ions (for instance, Ar^+ monoenergetic ions) strike the target surface and remove mainly neutral target atoms by momentum transfer, and these condense into thin film. At the same time, other particles such as electrons and negative ions are produced and accelerated towards the substrate and bombard it as shown in Fig. 5.2. In some instances, a bias potential, usually negative, is applied to the substrate holder, so that the growing film is subject to positive ion bombardment during film growth in a glow discharge environment. Effects of ion bombardment on surfaces of the grown film are important for physical and chemical properties.

CHAPTER 6

PLASMA POLYMERIZATION

Plasma polymerization refers to the formation of polymeric materials under the influence of plasma (partially ionized gas). It is a new material preparation process and is not a kind of polymerization. The materials obtained by plasma polymerization are vastly different from conventional polymers and constitute a new kind of material. In plasma polymerization or glow-discharge polymerization, an organic compound (monomer) in the gas or vapor phase is introduced into a vacuum system and subjected to plasma conditions created by some kind of electric discharge.

When organic molecules are exposed to a low-power rf discharge, complex chemical and physical processes take place, resulting in the formation of a solid material, referred to as plasma-deposited polymer [27]. Thin films produced in this way are becoming important for wide ranging applications from reverse osmosis membranes to dielectric barriers in electronic device fabrication. Plasma polymerization leads to polymer film formation at low temperatures, e.g., at room temperature, on any substrate. It is one of relatively few processes which permits the formation of very thin uniform polymer films which conform to a substrate of any shape.

Plasma-polymerized materials generally differ in structure and properties from those produced by common polymerization techniques. During conventional polymerization, only special bonds of the monomer molecules are selectively opened which leads to the formation of chains, whereas during plasma polymerization, the material is built up by the reactions of various types of radicals created from the monomer molecules by energetic collisions in the discharge [28]. The chemical structure of the resulting film depends upon the discharge regime. The film may be a highly cross-linked and branched polymeric material containing a number of unsaturated radicals and

molecular groups different from the monomer ones. On the other hand, it has been pointed out that careful control of the plasma discharge can produce polymers with chemical structures similar to those of common polymers.

6.1 Mechanistic Aspects of Plasma Polymerization

Although the plasma polymerization is an extremely complex process involving the complicated chemical reactions of organic molecule with high energy electron and ions, it is generally agreed that monomer molecules introduced into plasma are activated into reactive fragments, which then recombine to form new chemical bonds [29]. The repetition of these activation and mutual recombination reaction of monomer molecules in a plasma possibly leads to the deposition of plasma polymer whose chemical structure consists of the randomly cross-linked covalent network.

In discussions of a possible mechanism of plasma polymerization, two general routes are usually considered. One is a chain propagation mechanism similar to the conventional polymerization and sometimes called plasma-induced polymerization. Another one is stepwise reactions leading to the deposition of solid is called atomic polymerization. In chain-growth polymerization a long-chain molecule is formed by a series of consecutive steps that is completed in a very short time (e.g., within a fraction of a second). In this case, the products are only final polymers. Unlike the case of step-growth polymerization, intermediate-size molecules can not be isolated. Consequently, the entire polymer formation can be considered an essentially one-step process.

When the chain-carrying species (e.g., the free radical) is expressed by M^* and the monomer by M , the chain-growth mechanism can be shown by [29]



The series of reactions expressed by Eq. (6.1) is the propagation reaction, and the reaction in which the chain-carrying species is lost is the termination reaction [(6.2)].

Plasma polymerization can be explained best by rapid step-growth polymerization suggested by Yasuda [29]. This can be represented by



Where N represents the number of repetitions of similar reactions. The overall polymerization mechanism based on the rapid step-growth principle is shown in Fig. 6.1.

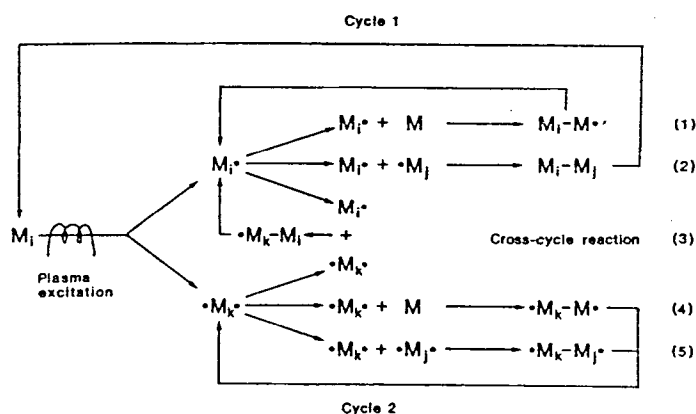


Figure 6.1 Schematic diagram of step-growth mechanism of plasma polymerization

In the Fig. 6.1 M_x refers to a neutral species that can be the original monomer molecule or any of the dissociation products. $M\bullet$ is a monovalent reactive species and difunctional activated species are shown by $\bullet M\bullet$. The subscripts i , j , and k merely indicate the difference in size of species involved. Step (1) and step (4) are essentially the same as the addition of reactive species to the monomer. Cycle 1 consists of reactions of monovalent reactive species and cycle 2 is based on divalent reactive species. Step (2) is a termination by the recombination mechanism. Step (3) is essentially a cross-cycle reaction from cycles 1 and 2 and step (5) is a combination of bifunctional intermediates, which may

play a major role in certain monomers under certain conditions. Cycle 1 requires the reexcitation of the product species, whereas cycle 2 can proceed without reexcitation as long as divalent reactive species exist. Any of the species involved will collide with the substrate surface, however, not all of them would remain on the surface, depending on the kinetic energy of impinging species. The deposition occurs when an impinging particle fails to leave the surface by loss of kinetic energy or by formation of a chemical bond.

Many reactions occur simultaneously in a plasma polymerization system. From the viewpoint of plasma polymerization as a material production process, there are two opposing processes: polymer formation, which leads to the deposition of material, and ablation, which leads to the removal of material. The overall scheme of plasma polymerization (Fig. 6.2) [29] encompasses the principle of the competitive ablation and polymerization mechanism.

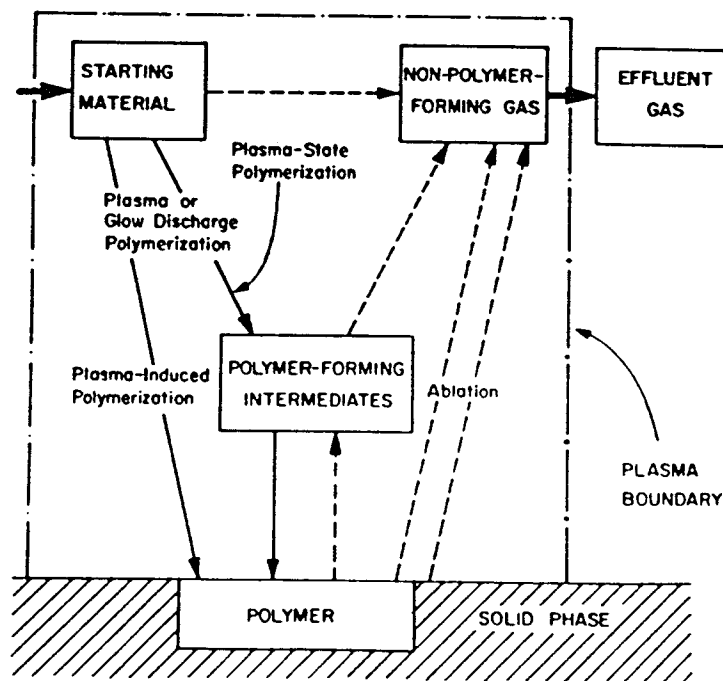


Figure 6.2 Overall scheme of polymerization in glow discharge

The ablation process associated with monomer can be visualized as the splitting of a molecule or the fragmentation of the monomer. This aspect is very important in plasma polymerization, and it is not an exaggeration to state that no monomer polymerizes without fragmentation in plasma. The main route of polymer formation occurring under the influence of plasma is via plasma-state polymerization (Fig. 6.2); the possibility of plasma-induced polymerization always exists, however.

6.2 Parameters Involved in Plasma Polymerization

Parameters which define the system, such as monomer flow rate and pressure of the system, as well as parameters of discharge such as discharge power (or current density and voltage), frequency of the excitation signal and distance between electrodes, etc., are obviously important parameters for describing and controlling the experimental conditions of plasma polymerization and the deposition rate.

The rate of polymer deposition has been found to have a monotonic rise at first as the flow rate of monomer is increased at a constant power and pressure because the polymerization rate is limited by the supply of fresh monomer. At high flow rates the deposition rate decreases as the residence time of the monomer is lowered and even activated species may be prevented from reaching the substrate by being drawn away and pumped out. A maximum occurs where competing processes are balanced [30].

When pressure and flow rate are held constant the deposition rate generally increases with power (power density) and becomes independent of power at high values. The effect of pressure is similar. The deposition rate rises at first and tends to saturate at increased pressure (power and flow rate being held constant). It has also been observed that the deposition rate can be increased by cooling the electrodes. The dependence of the rate on source frequency has not been ascertained.

6.3 Structure and Properties of Plasma Polymer Films

The structure of plasma polymerized films and their properties are strongly influenced by the deposition parameters. At high pressures and flow rates an oily film (less cross-linked) is deposited. At a low pressure and high flow rate a hard, pinhole-free and transparent film is obtained, but when the flow rate is decreased a 'powder' is produced which means that plasma polymerization also takes place in gas volume. At a relatively low input energy level W/F_m (W is the discharge power and F_m is the mass flow rate of monomer), a plasma polymer is obtained whose structure and properties are very similar to those of polymer. However, with increasing W/F_m , the chemical structure changes gradually to the more dense covalent network with less organic groups. The uniqueness of plasma polymer consists in this controlled chemical structure which lies somewhere between the polymeric and inorganic materials. Investigations from AES and ESCA show that, in general, plasma polymerized films contain more carbon than corresponding conventional polymers and some impurities, e.g., oxygen and nitrogen.

In general, the properties of polymeric films synthesized in plasmas may be summarized as follows. Films are amorphous, pinhole-free and highly cross-linked. Because the resulting polymer film has many chemical bonds, the films are generally chemically inert, insoluble, mechanically tough, thermally and chemically stable, have high melting points and have been used in a wide variety of applications such as permselective membranes, protective coatings, and electrical and biomedical films.

CHAPTER 7

EXPERIMENTS

7.1 Polymer Film Fabrication Method

In this section experimental setup and deposition procedure for plasma polymerization has been discussed.

7.1.1 Experimental Setup for Plasma Polymerization

The RF plasma reactor system used in these studies is illustrated in Fig. 7.1. The system consists of the following units:

A vacuum chamber (Bell-Jar type) made of pyrex-glass and a pair of internal copper electrodes. A mechanical pump is used to develop pressure down to 10^{-3} Torr and diffusion pump to get high vacuum. Flow meters control the flow of Ar and monomer. There is a thermocouple gauge to measure chamber pressure during deposition and ionization gauge to measure backing pressure. Finally a RF generator is used for high voltage supply.

7.1.2 Substrate Preparation

Micro-slide glasses $3.7\text{cm} \times 2.5\text{cm} \times 0.1\text{cm}$, were used as substrates in these experiments.

The samples were cleaned by using the following steps:

- 1) Wash with detergent
- 2) Keep 5 min in Ultrasonic cleaner
- 3) Keep 5 min in Acetone
- 4) Keep 5 min in Methanol
- 5) Finally wash with deionized water

6) Dry the sample with high pressure jet of clean oil-free nitrogen which blows the liquid off the surface rapidly.

7.1.3 Monomer Preparation

Methylmethacrylate (MMA) was used as a base monomer in our experiments. Usually a small amount of inhibitor is added to the monomer to prevent polymerization during shipment and storage. Prior to polymerization this inhibitor should be removed. It was filtered by passing it through a long tube filled with De-hibit 100 ion exchange resin. The monomer was passed at a rate of 1 drop/sec. After removing the inhibitor, monomer container should be kept in dark place to prevent monomer cross linking depicted by color change.

7.1.4 Polymer Deposition Procedure

The apparatus for plasma polymerization used in this experiment is shown in Fig. 7.1. The system consisted of a 14 cm diameter \times 42 cm deep pyrex-glass cylinder, a vacuum system and a gas inlet system. Inside the reaction chamber two parallel (4.5cm \times 4.5 cm) copper electrodes, one containing the excitation electrode and another grounded electrode which holds the substrate on it, were located as shown in the Fig 7.1. They were separated 3 cm apart. Plasma was generated in a capacitively coupled radio frequency generator operating at a fixed frequency of 13.56 MHz with a maximum output of 1.2 KW.

Before polymerization the system was pumped by an oil-diffusion pump down to $\sim 10^{-6}$ Torr. This was backed up by a mechanical pump. Pressure measurement was carried out using (Veeco TG-7) thermocouple gauges. The chamber was then flushed with Argon gas twice to eliminate moisture adsorbed on the surfaces of the substrate and chamber wall. The system was evacuated again and then monomer gas was fed for 10 minutes to get a steady state flow. Argon at the flow rate of 65 cm³ /min (STP) was used

as a carrier gas and its flow rate was controlled by means of a (MKS - 1259) flowmeter. The monomer and argon gases were supplied to the chamber by leak valves and the pressure was recorded by means of a thermocouple gauge (Fig. 7.1). The flow rate of monomer vapor was adjusted to $22 \text{ cm}^3 / \text{min}$ (STP) by a micrometering valve. The chamber pressure was 500 mTorr during deposition.

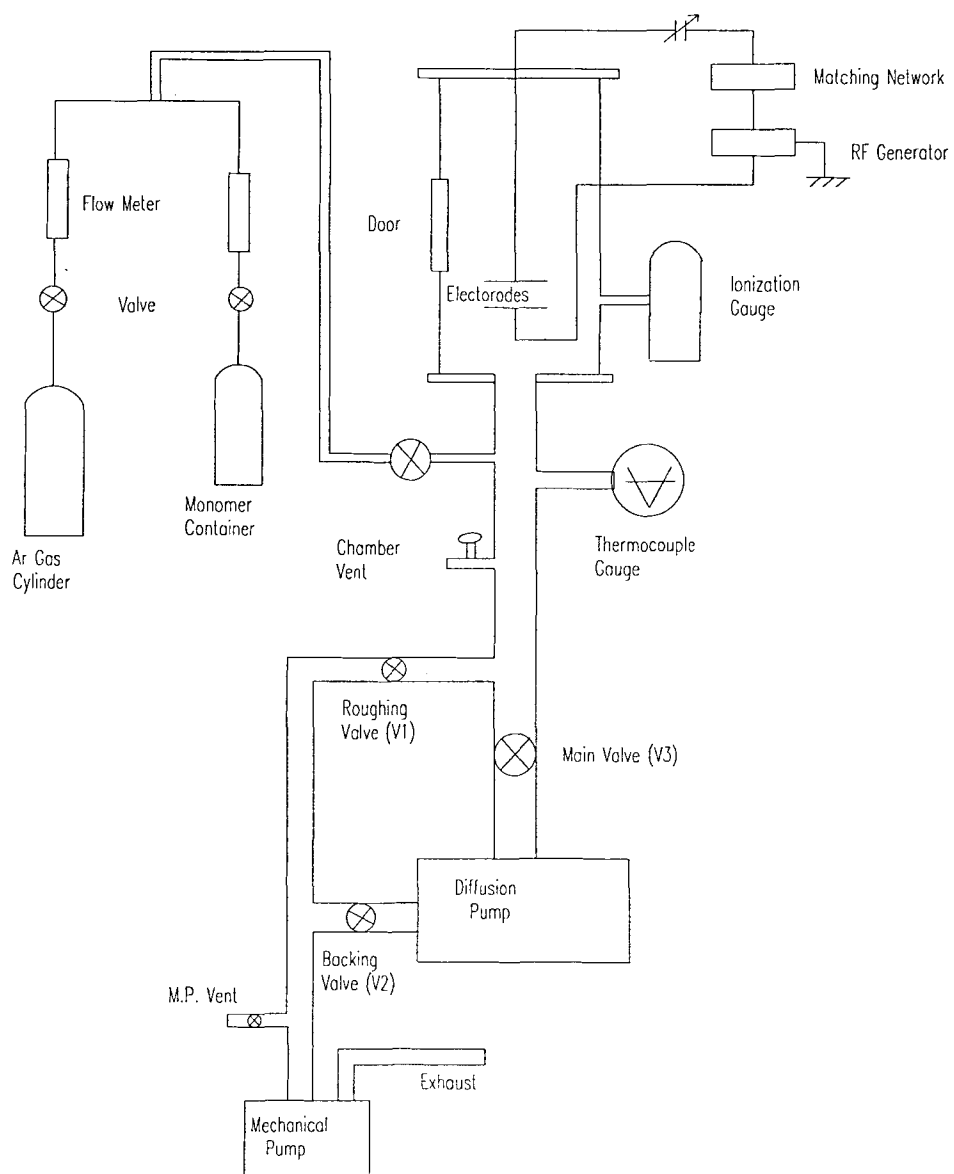


Figure 7.1 Schematic diagram of rf sputtering system

Following the stabilization of flow rate, glow discharge was initiated and continued for desired time at a fixed discharge power of 25 W. In all experiments the discharge conditions, such as gas flow rates, rf power, frequency and position of the substrates within the chamber, were kept constant (Table 7.1). The only variable in this experiment was the deposition time.

7.1.5 Thickness Measurement

The mass of the films was calculated by weighing the glass substrates before and after depositions. The weight of the film (ΔW) was about 0.11×10^{-3} gm for 10 minutes of deposition. The film thickness was measured from dividing the weight difference ΔW by the area of the sample and by the density. The density of PMMA was 1.2 g/cm^3 . The thickness was verified by depositing the film on a silicon wafer and deducing the film thickness by using Ellipsometry method.

Table 7.1 Conditions Used for Depositing Plasma Polymerized Films of MMA

Background Pressure	9×10^{-6} Torr
Pressure with monomer	270 mTorr
Pressure with Ar	350 mTorr
Total pressure	500 mTorr
Flow rate of monomer	22 SCCM
Flow rate of Ar	65 SCCM
Total flow rate	77 SCCM
Interelectrode distance	3 cm
RF power	25 watt
Deposition time	2, 5 min
Maximum rate of deposition	$100 \text{ \AA} / \text{min}$

7.2 Metal Cluster Fabrication Method

The incorporation of metal particles into hydrocarbon polymer films produced by plasma techniques is an attractive prospect. It is visualized that careful choice of metal and organic phases, and close control of the overall composition of the product, would greatly extend the scope of these plasma polymerized materials in, for example, electrical, mechanical, magnetic, and optical applications. Many discharge configurations are being explored for various etching and polymerization applications. The rf capacitively coupled, diode systems appear to be emerging as the most reliable and flexible to meet many of the technological needs [26]. Furthermore, the broad experience gained of this configuration from the much more mature sputtering technology provides considerable insight into the significance and control of the relevant discharge parameters.

7.2.1 Experimental Procedure

A typical reactor configuration used for this work is a capacitively coupled diode arrangement in which one electrode (anode) is at ground potential. A plasma generated in a Ar gas mixture is excited by means of 13.56 MHz radiofrequency power applied to the other electrode (cathode), i.e. the excitation electrode, whose surface consists of the metal to be incorporated into the polymer film. At this frequency the excitation electrode attains a relatively large self-biasing negative potential, relative to the plasma. Positive ions, therefore, arrive at the target surface with sufficiently high kinetic energy. In such a configuration, the powered electrode, in our case Au, Ni and Si target is submitted to intense positive ion bombardment, which leads to the removal of atoms from the target by physical sputtering.

The system used for sputtering is described in article 7.1.4. Gold and Nickel target of 4cm × 4cm were used in this experiment, whereas, Si target was 5.5 cm in diameter. Prior to deposition the system was evacuated to a pressure of $\sim 10^{-6}$ Torr by the use of a mechanical pump and diffusion pump (Edwards Vacuum Inc.). The pressure was

measured by a 843 Varian Ionization gauge in the absence of the discharge. The presence of the discharge obviously alters the system pressure, but this pressure could not be measured using the ionization gauge due to rf interference. Ar gas was injected into the discharge system with a Av. flow rate of 22 SCCM and the flow rate was controlled by a MKS-1259 flowmeter. During deposition the pressure was kept constant at 10-25 mTorr while the background pressure was 9×10^{-6} Torr. In order to get cluster deposition rather than uniform deposition some process parameters like system pressure, flow rate, discharge power etc. (Table 7.2) were adjusted. Before deposition the chamber was washed twice with Ar gas to remove moisture and monomer adsorbed on the chamber wall.

Table 7.2 Summary of Process Parameters For Metal Cluster Deposition

Sample No	Materials Used	Pressure (mTorr)	Ar Flow (SCCM)	rf Power (Watt)	Bias Voltage	Time of Deposition	Av. Cluster Size (D)
1	Gold	25	5	80	450	15 sec	60 Å
2	Gold	25	5	80	450	30 sec	300 Å
3	Gold	25	5	80	450	45 sec	500 Å
4	Nickel	20	5	140	600	7 min	40 Å
5	Nickel	20	5	140	600	9 min	50 Å
6	Silicon	10	30	270	750	12 min	not found

Also, there is always formation of polymeric films at the surface of the metal target. In order to remove polymer deposit, the metal target should be submitted to high-energy ion bombardment by Ar^+ . This approach keeps the target clean and available for metal sputtering. This is readily achieved by using a total power of 150-200 W in the discharge. After cleaning the target, and after a steady state condition is reached, the substrates were exposed to Ar plasma at a rf power of 100-300 W (bias voltage 450-750 V) for metal or Si deposition. The substrates were kept under vacuum for 15 min after deposition.

Vacuum in the chamber was released by flowing air and the substrates were removed from the chamber. The average deposition rate under these conditions was 10-50 Å/min. In this experiment multilayer systems (polymer/metal sandwich) were investigated. Optical transmittance were recorded with a Spex 1681 Minimate-2 single-beam spectrometer. A very thin layer (~150 Å) was deposited on NaCl crystal and then removed from the substrate for Transmission Electron Microscopy (TEM) analysis. The electron diffraction pattern were taken at the same time.

7.2.2 Transmission Electron Microscopy (TEM)

A number of samples for TEM observation were prepared by depositing directly onto NaCl crystal, which was subsequently dissolved in water. NaCl dissolves in water leaving the thin films floating on water. The stripped thin films were then picked up carefully with a copper mesh and used as specimens for TEM observations. The films were investigated with a Philips 400 T electron microscope operating at 120 KV and its resolution was about 2 nm. The magnification used was 100,000-280,000. The measurements were done at Stevens Institute of Technology by Dr. Yan Opyrchal. For gold samples TEM was performed in bright-field mode, whereas, for Ni samples TEM was taken in a dark-field mode. A dark-field mode is the illumination of an object in a microscope in such a way that only light diffracted by the objects reaches the eye. It is applicable only to the examination of very small particles, which appear as bright images against a dark background. In a bright-field mode particles appear as dark images against a brightly lighted background.

7.2.3 Determination of Metal Volume Fraction x

The gold volume fraction x has been computed from TEM micrographs (Fig. 8.1) by calculating different sizes of clusters and their volumes. For Ni, volume fraction has been determined from the cluster mass by weighing the samples before and after deposition

and from the film volume obtained by area computation and polymer thickness measurement.

7.3 Optical Measurement System

7.3.1 Experimental Setup

Experimental configuration is shown in Fig. 7.2

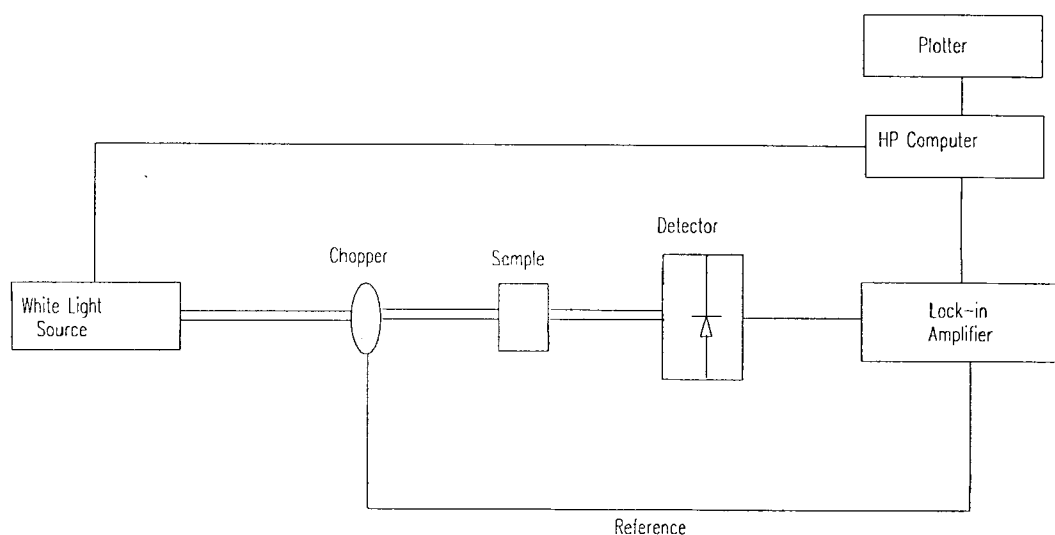


Figure 7.2 Optical measurement system

The experimental arrangement, which allowed measurements of transmittance at different wavelengths, consisted of a 100 W white-light source with a monochromator, a compudrive, and a detector connected to a lock-in amplifier system. The white light beam provided by Spex 1681 spectrometer passes through the sample which is detected by a detector. A Spex CD2A compudrive is used which has total keyboard control over the spectrometer and it is connected to a HP computer for two way communications. The Model SR540 optical chopper which provides a reference frequency to the lock-in amplifier (Model SR510) increases the signal-to-noise ratio. The lock-in amplifier is used

to detect and measure the signal with a reference frequency provided by the chopper. The frequency of the optical chopper is chosen not to be the line frequency and all its even and odd harmonics should be carefully avoided. The output of the lock-in amplifier is converted to digital signal and sent through a IEEE-488 interface to the HP 300 computer.

7.3.2 Computer Program for Data Collection

The model SR510 lock-in amplifier and Spex CD2A computer have the GPIB interface. They were connected with a HP 300 computer's I/O. A program written in BASIC language (see appendix B) was used to store the data from the lock-in amplifier to the computer.

7.3.3 Transmittance and Reflectance Measurement

The normal-incidence optical transmittance for the discontinuous metal and Si films were recorded for wavelengths between 300 and 1600 nm by using a Spex 1681 single beam spectrometer. The reflectance of the samples were measured from 300 to 700 nm at 45° incidence. The samples were normalized to the transmittance and reflectance of a PMMA coated glass substrate. In this way the influence of the polymer layer can be diminished significantly. In order to simulate the experimental transmittance spectra, a versatile computer program was written and the data were recorded by a HP-300 series computer from the lock-in amplifier.

CHAPTER 8

EXPERIMENTAL RESULTS

8.1 Characterization of the Metal-Free Polymer Films

Polymer films formed on the substrates have complex, highly cross-linked, and amorphous structures. Polymer film formed by glow discharge is highly dependent on the system and the conditions under which the polymer is formed. In order to achieve higher deposition rate and high quality film, some process parameters like system pressure, flow rate, discharge power and the distance between two electrodes were adjusted (Table 7.1). We noticed that deposition rate generally increases with power under constant pressure and flow rate but if high power is used, the film tends to become brittle and discolored (yellowish).

8.1.1 Deposition Rates

Deposition rates of plasma polymer were examined in terms of time. It was found experimentally that polymer deposition rate increases initially with time and after certain time it starts to decrease.

8.1.2 Refractive Index

The refractive index of plasma polymer was evaluated by Rudolph Research/Autoel ellipsometer. Refractive index of plasma PMMA was higher than the index of conventional polymer films [25].

$n = 1.527$ for glow discharged PMMA

$n = 1.50$ for conventional polymer films

8.1.3 UV-Visible Spectra

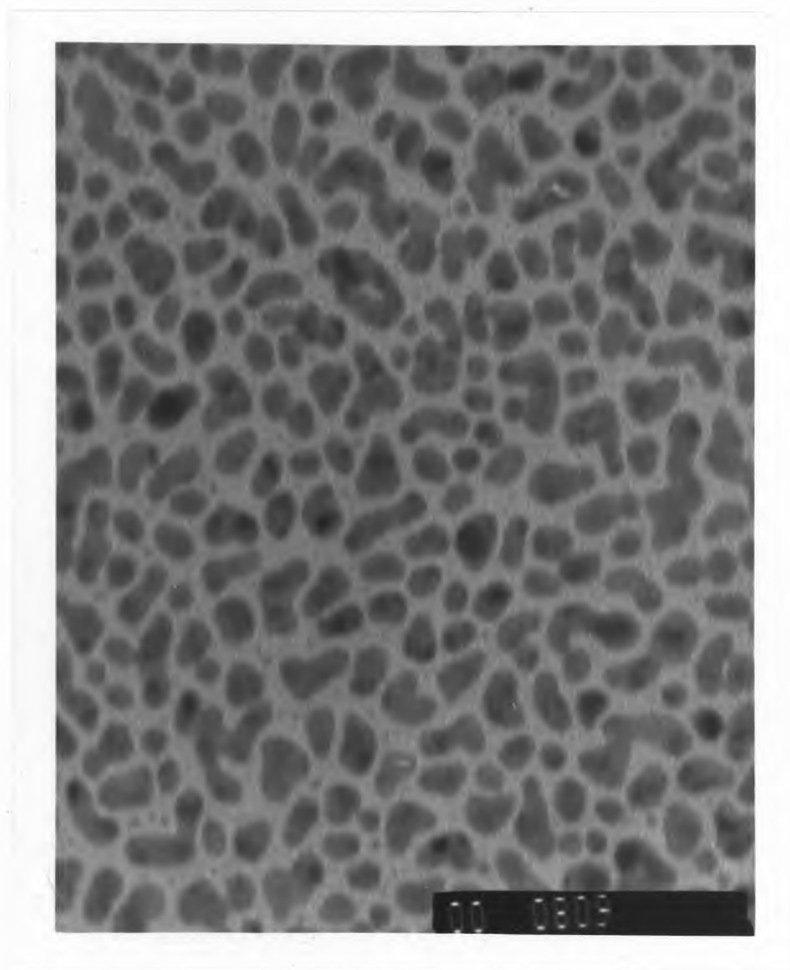
UV-Visible transmission were measured with a Model 1681 Minimate-2 spectrometer in the wavelength range of 300-1000 nm. Fig. A.9 shows UV-Visible transmission curve for 10 minutes deposited polymer film.

8.2 Structural Analysis of the Metallic Phase by TEM and Electron Diffraction

The shape and size of the metal clusters has been performed as a function of the metal volume fraction x by TEM analysis.

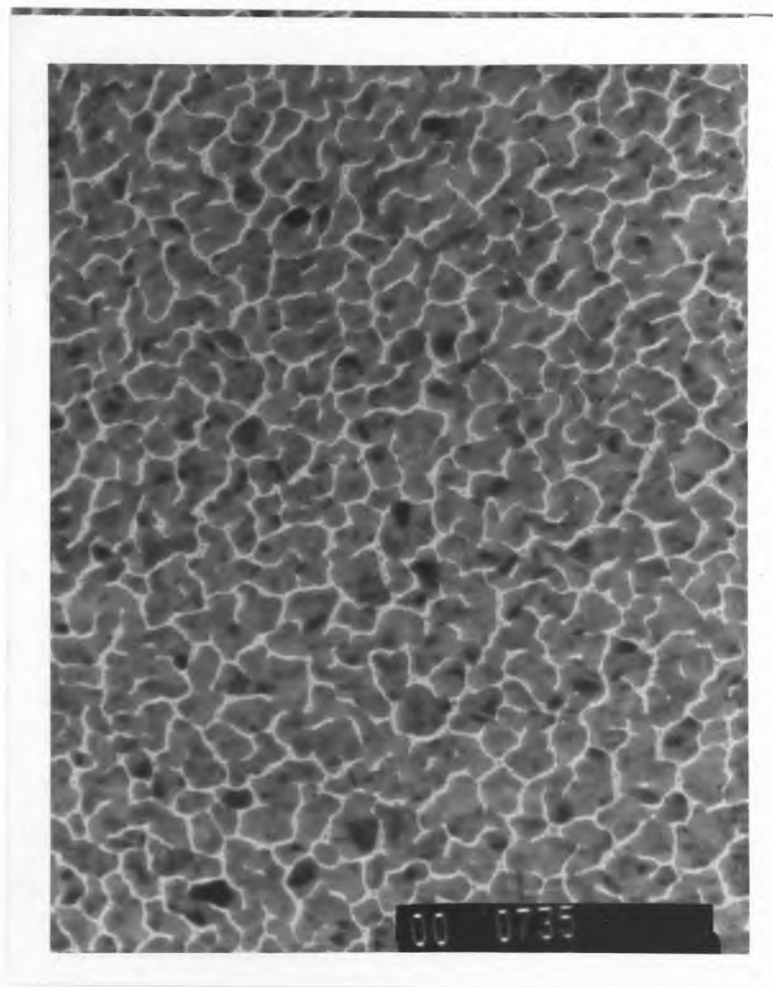
8.2.1 Gold-Containing Samples

In Fig. 8.1, 8.2, A.3 and A.4 (Appendix A) a few TEM pictures of low and high gold volume fraction (x) films are presented. At low x , the gold clusters appear roughly spherical and isolated from one another as shown in Fig. 8.1. For low gold contents the clusters have a mean diameter of 3-10 nm. It is obvious from the micrographs of Fig. 8.1 that the distribution of the clusters reasonably homogeneous in the plane of the film. By increasing the sputtering time, the ellipticity of the particles is increased. It is clear from Fig. 8.2 that when x is increased the average size of the clusters as well as their irregularity is enhanced and wormlike gold cluster is developed. At high x , gold clusters are already interconnected as shown by Fig. A.3. A cluster-size distribution histogram for low x ($x = 0.05$) is presented in Fig. 8.3. The electron diffraction pattern (Fig. A.4) of polycrystalline gold clusters does not reveal any morphological difference between cluster and bulk gold. The distances between the concentric circles are comparable to the lattice parameter of gold. Properties of several gold island films are summarized in Table 8.1.



|-----|
200 Å

Figure 8.1 TEM micrographs of 15 sec deposited gold particles [$x = 0.05$]



|-----|
500 Å

Figure 8.2 TEM micrographs of 30 sec deposited gold particles [$x = 0.10$]

8.2.2 Nickel-Containing Samples

Micrographs were taken for samples corresponding to nickel volume fractions of $x = 0.13$ (7 minute nickel) and $x = 0.17$ (9 minute nickel) as shown in Fig. 8.4 and A.7. TEM micrographs of Fig. A.8 is not clear. It can be seen that as in the case of gold, the nickel clusters are roughly spherical and isolated for low volume fractions. It is seen from the micrographs that the average size of the nickel clusters is smaller than the gold clusters. Fig. A.8 (Appendix A) shows the electron diffraction pattern of 9 minute nickel.

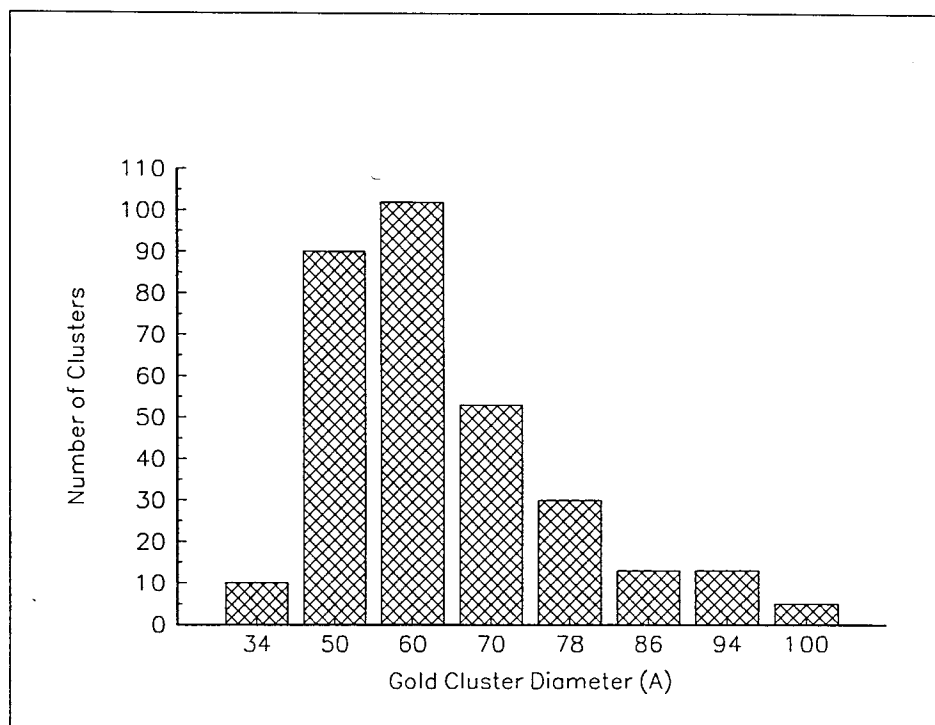


Figure 8.3 Distribution of the number of gold particles as a function of gold cluster diameter from the TEM picture of Fig. 8.1

Table 8.1 Properties of Island Films of Gold

Film No.	Deposition time (sec)	Volume Fraction (x) %	Max Absorption Wavelength (nm)	Film Thickness (Å)
1	15	5	660	13
2	30	10	760	25
3	45	15	840	37
4	60	20	870	50
5	90	30	980	75

8.2.3 Silicon-Containing Samples

For silicon samples no visible TEM micrographs could be achieved. The reason is the very close atomic numbers of both silicon and polymer (oxygen and carbon) matrix. There should be a significant difference in atomic numbers in order to separate clusters from matrix in TEM micrographs.

Table 8.2 Properties of Nickel Islands

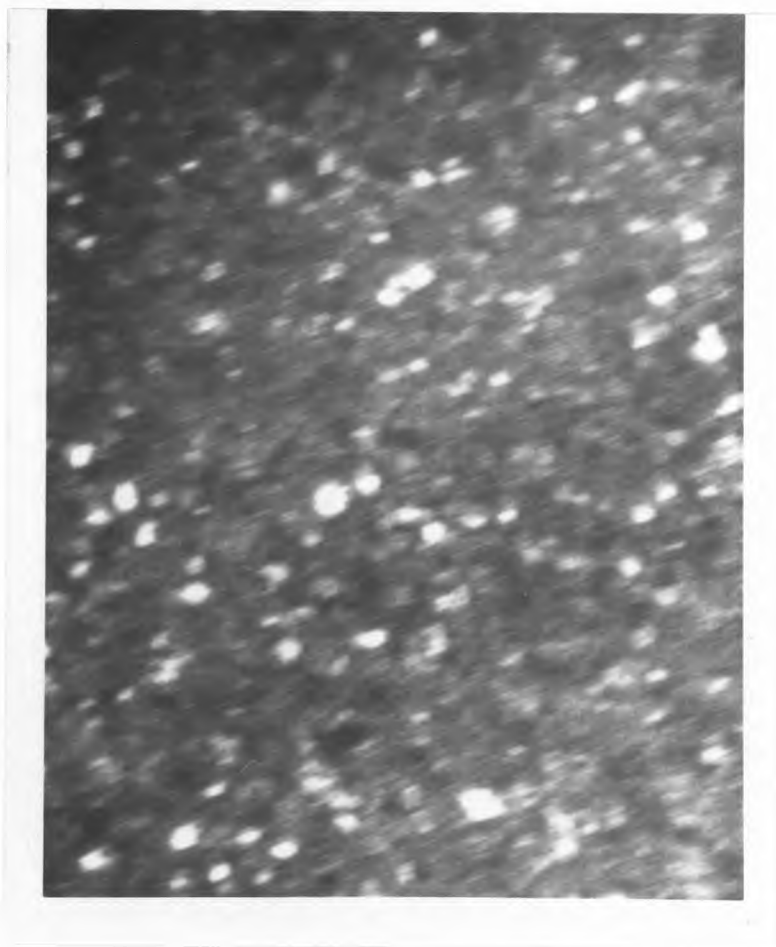
Film No.	Deposition Time (min)	Volume fraction (x) %	Max. Absorption Wavelength (nm)	Film Thickness Å
1	10	18	350	120
2	20	37	340	240
3	30	55	340	360
4	40	74	350	480
5	60	100	350	720
6	80	100	360	960
7	95	100	380	1140

8.3 Analysis of Optical Transmittance Spectra

8.3.1 Gold Films

The optical transmittance spectra in normal incidence for 6 gold films (multiple gold/polymer layers) are presented in Fig. 8.5-8.8, 8.10 and A.6 (Appendix A). In general, all the curves are characterized by an absorption band in the visible region and higher transmission in near infrared region and a very small absorption peak in the UV region (Fig. A.6). Fig. 8.5 and 8.6 show transmission curves of 6 layers of gold each 30 sec separated by 5 and 2 minute (min) polymer. Samples with 2 min polymer exhibits a little wider absorption maxima than of 5 min polymer. Similar phenomena is observed when we look at Fig. 8.7 and 8.8 which represent 6 layers of gold film each 1 min separated by 5 and 2 min polymer.

Fig. 8.10 exhibits transmittance spectra of five gold samples (without polymer) for different deposition time. It is noticed from Fig. 8.10 that absorption maxima depends on the deposition time and this is shown graphically in Fig. 8.9. Fig. A.5 represents transmittance spectra of gold clusters of five different thicknesses deposited on glass substrates by ultrahigh-vacuum [3]. In Fig. A.6 curve 1 shows six layers of gold, each 30 sec, separated by 2 min polymer. Whereas curve 2 represents six layers of gold, each 1 min, separated by 5 min polymer.



|-----|
300 Å

Figure 8.4 TEM micrographs of 7 min deposited nickel particles [$x = 0.13$]

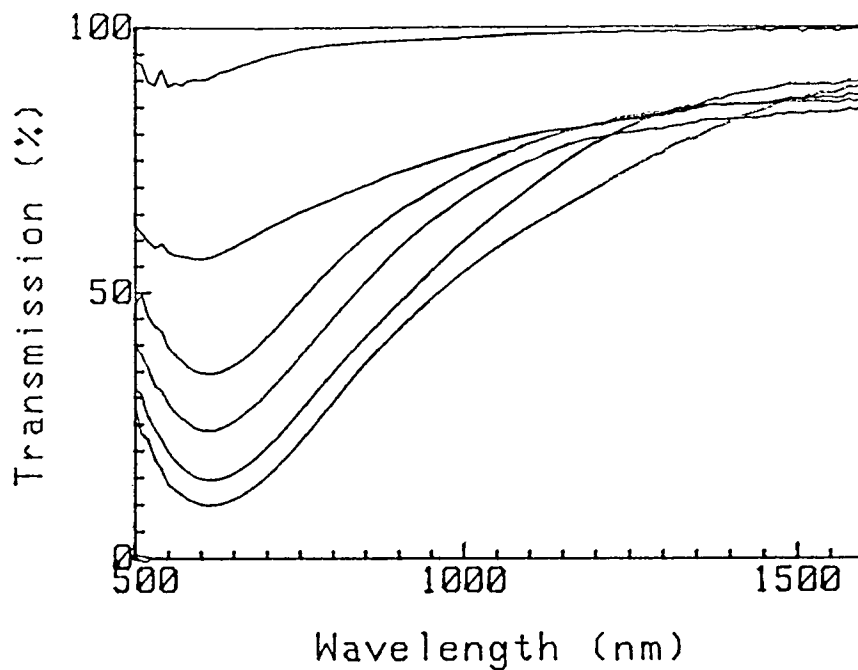


Figure 8.5 Normal transmittance of successive gold/polymer layers. Deposition time: Gold -30 sec, Polymer-5 min. Top curve-1st layer, Lowest curve-6th layer

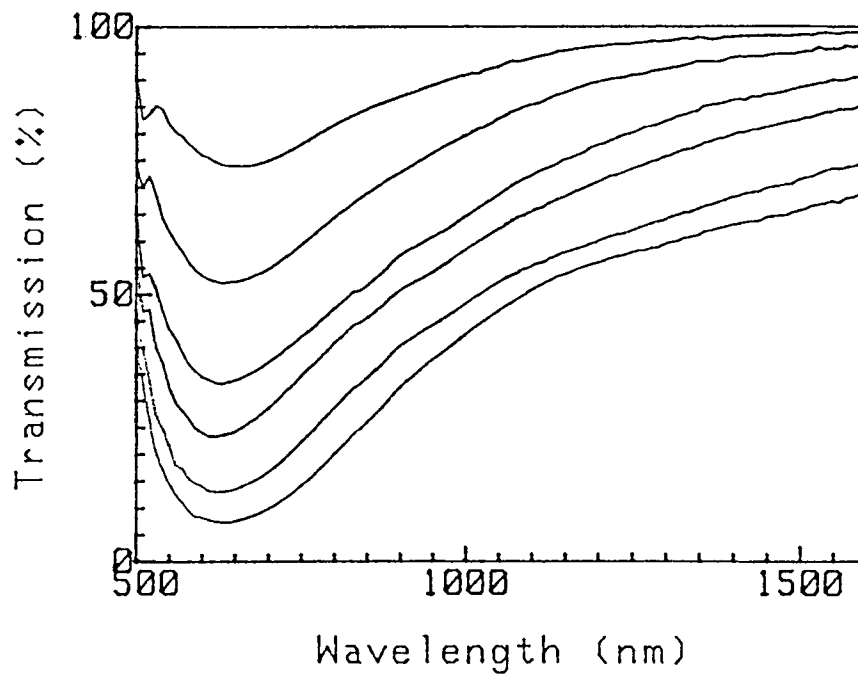


Figure 8.6 Normal transmittance of successive gold/polymer layers. Deposition time: Gold -30 sec, Polymer-2 min. Top curve-1st layer, Lowest curve-6th layer

8.3.2 Nickel Films

Transmittance spectra for normal-incidence optical beam were measured for nickel cluster films in the wavelength range of 300-1000 nm as shown in Fig. 8.11, A.1 and A.2. Fig A.1 (Appendix A) exhibits 6 layers of nickel (successive nickel/polymer layers) where the deposition time of each nickel layer was 10 min, much higher compared to 0.5 and 1 min gold. The spectra are characterized by an absorption peak in the UV region and a higher transmittance in the near infra-red spectral region.

Fig. 8.11 shows transmittance spectra for one layer of nickel for different deposition time. Fig. 8.12 depicts the change in absorption peak with deposition time. Fig. A.2 shows three layers of nickel, each 12 min separated by 5 min polymer. Three layers of nickel look more lossy than 6 layers of nickel (Fig. A.1).

8.3.3 Silicon Films

Transmittance for normal-incidence optical beam were measured for silicon films in the wavelength region of 300 - 1000 nm. The transmittance spectra for silicon samples are shown in Fig. A.10 - A.12. An absorption peak is observed in the UV region around 380 nm for all of the samples. Fig. A.10 shows the spectra of two silicon samples prepared by two different sputtering system for 30 minute (min) deposition (no polymer). They both have similar absorption peak in the UV region. Fig. A.11 shows two curves, one is 3 layers and another is 6 layers of silicon, each 12 min, both separated by 5 min polymer. For 6 layers of silicon, absorption peak in the visible region has shifted to the longer wavelength, while it remains at the same position in the UV region. In Fig. A12 transmittance curve 1 is the same one as described in Fig. A11. Curve 2 represents 4 layers of silicon and curve 3 represents 3 layers of silicon, each 6 min separated by 5 min polymer. It is noticed that there is no absorption peak in the visible region for 6 min silicon.

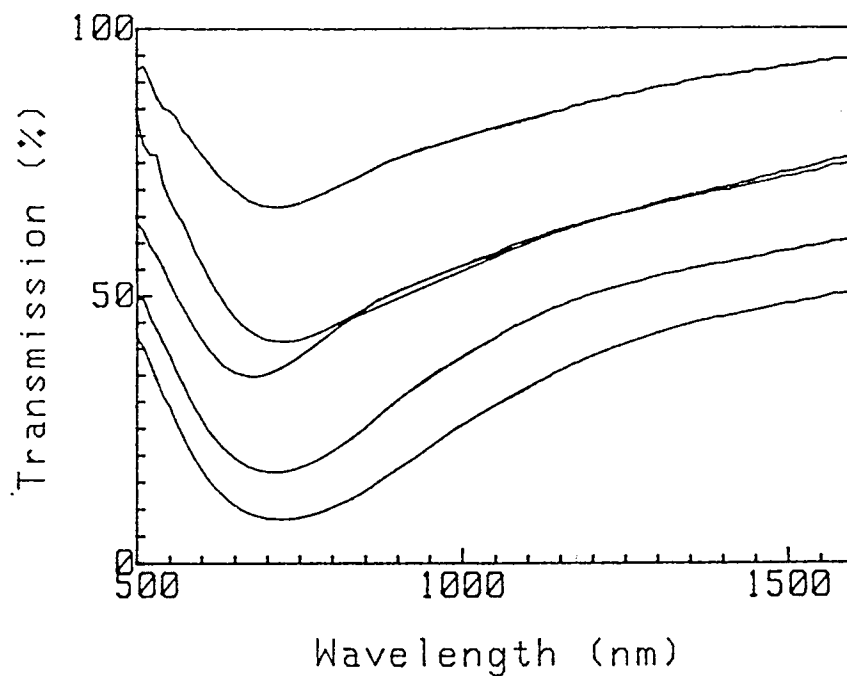


Figure 8.7 Normal transmission of successive gold/polymer layers. Deposition time: Gold-1 min, Polymer-5 min. Top curve-1st layer, Lowest curve-5th layer

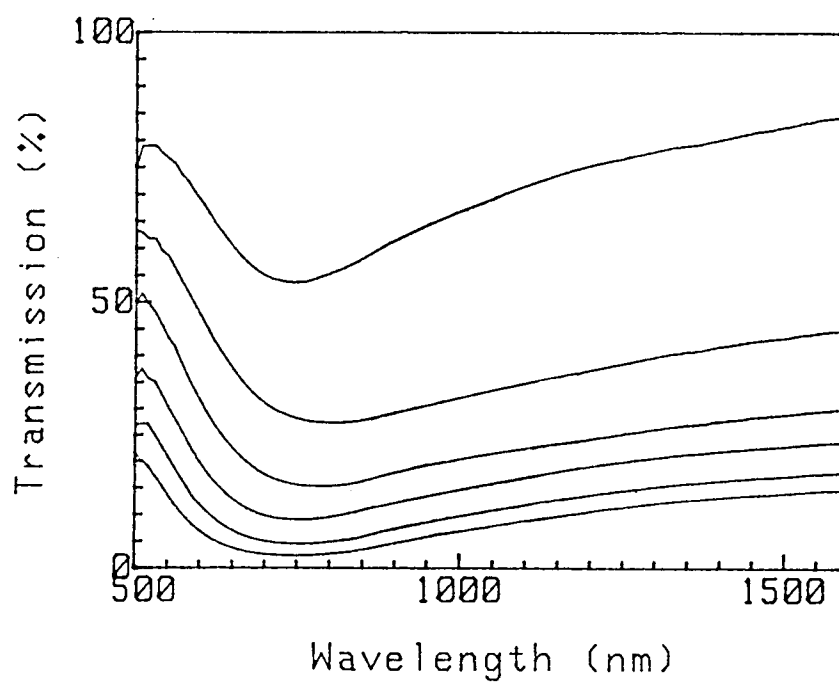


Figure 8.8 Normal Transmittance of successive gold / polymer layers. Deposition time: Gold-1 min, Polymer-2 min. Top curve-1st layer, Lowest curve-6th layer

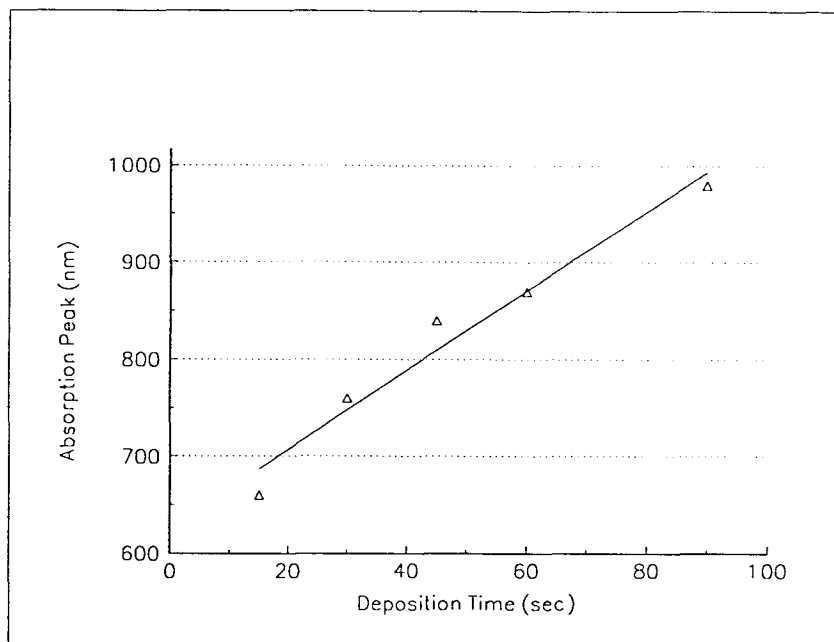


Figure 8.9 Variations of absorption peak with deposition time for various gold films

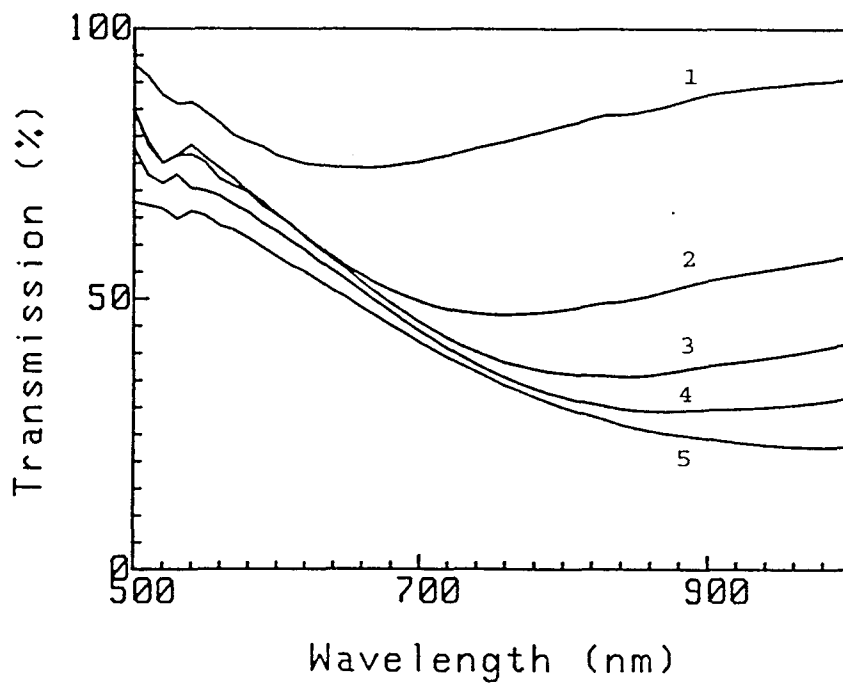


Figure 8.10 Normal transmittance curves of gold samples for different deposition time. The deposition time of each film is given in Table 8.1

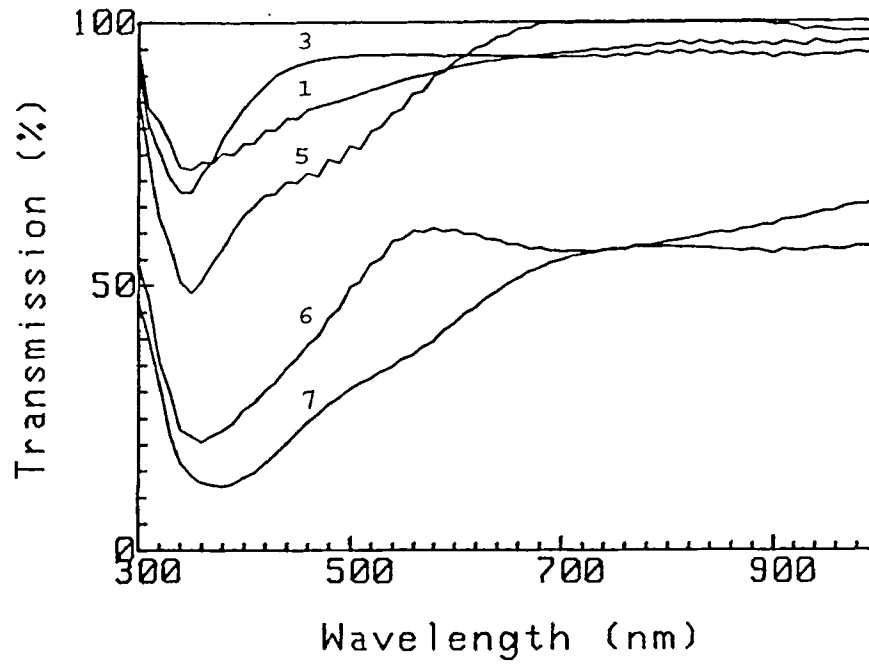


Figure 8.11 Normal transmittance curves of one layer of nickel for different deposition time. Deposition time of each layer is given in Table 8.2

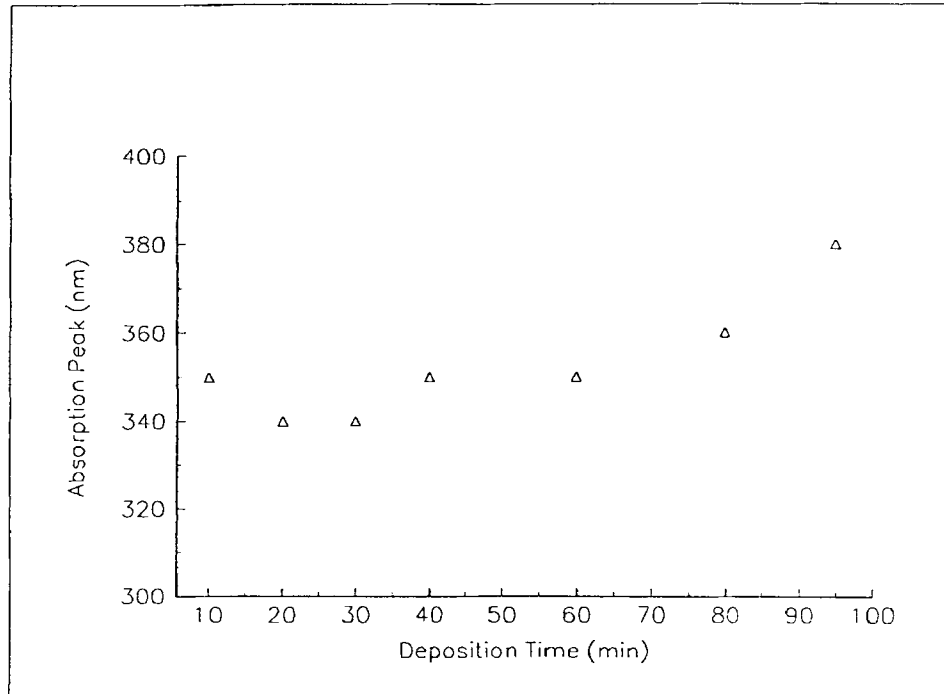


Figure 8.12 Variations of absorption peak with deposition time for various nickel films

8.4 Analysis of Transmittance and Reflectance Spectra at 45° Incidence

Optical transmittance and reflectance at 45° incidence were measured for gold, nickel and silicon films in the wavelength region of 300 - 700 nm as shown in Fig. 8.13 - 8.15. Fig. 8.13 shows a transmittance minima and reflection maxima at 680 nm for gold sample. Fig. 8.14 exhibits minimum in transmission at 380 nm and maximum in reflection at 360 nm for nickel sample. A minimum in transmittance at 350 nm and maximum in reflection at 370 nm is observed in Fig. 8.15 for silicon sample.

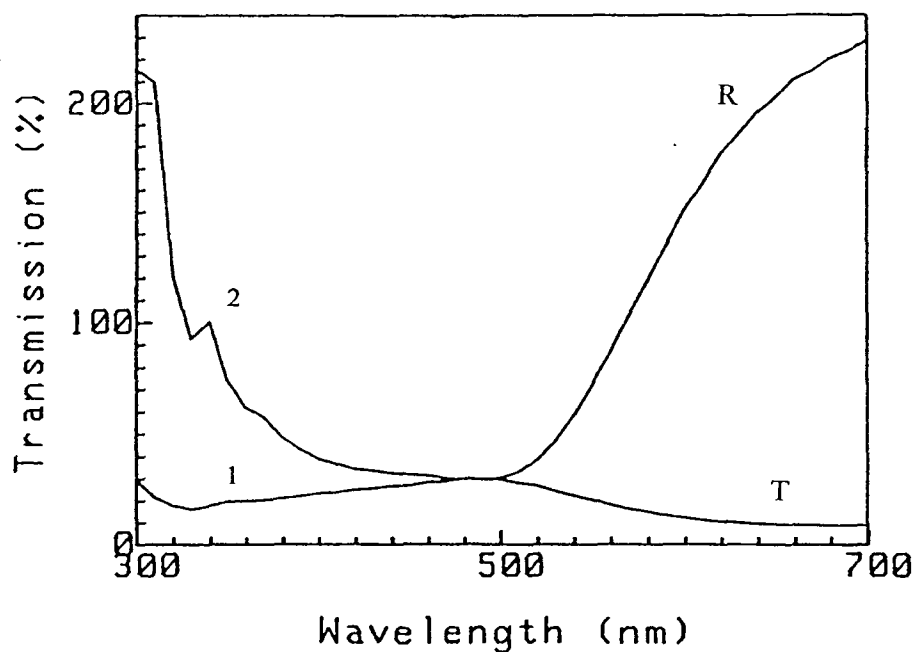


Figure 8.13 Transmittance and reflectance curve of 6 layers of gold at 45° incidence. Deposition time: Gold-15 sec, Polymer-2 min. Curve (1): Transmittance (2): Reflection

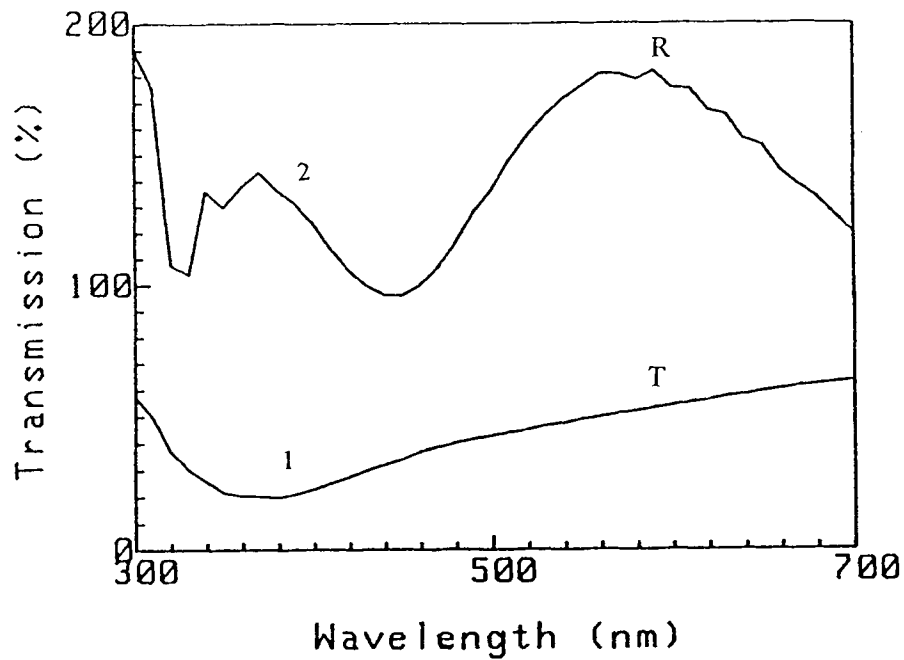


Figure 8.14 Transmittance and reflectance curve of 6 layers of nickel at 45° incidence. Deposition time: Nickel -10 min, Polymer-2 min. Curve (1): Transmission (2): Reflection

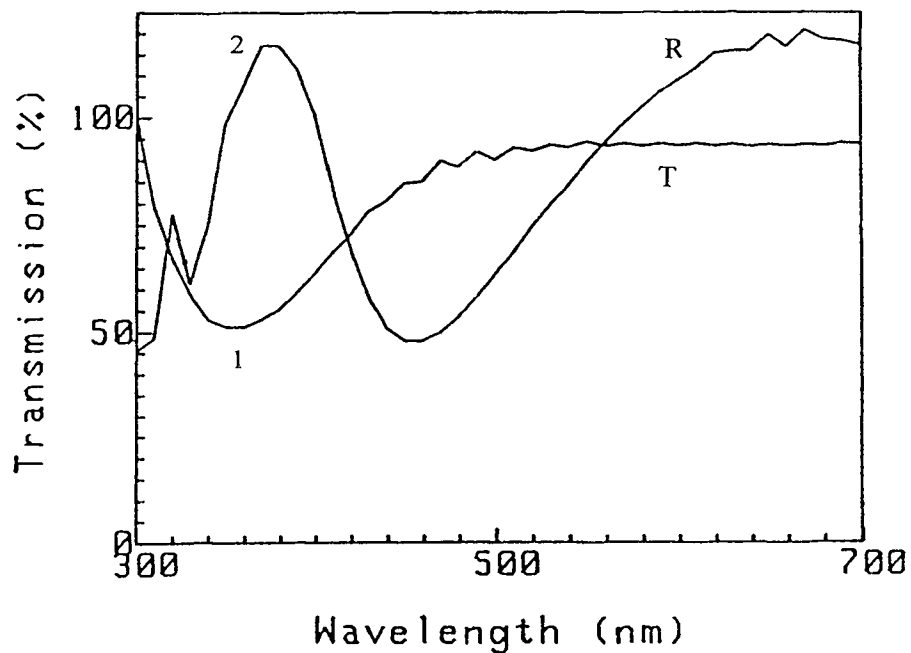


Figure 8.15 Transmittance and reflectance curve of 3 layers of silicon at 45° incidence. Deposition time: Silicon-6 min, Polymer-5 min. Curve (1): Transmission (2): Reflection

CHAPTER 9

DISCUSSION

In this thesis plasma polymer matrix was used as a substrate for gold, nickel, and silicon cluster fabrication. Polymer films produced by a glow discharge often possess chemical and physical properties which are different than conventional polymerized materials. The relationship between the deposition rate of plasma polymerized MMA (Methyl Methacrylate) over time showed an initial rate increase and after a certain time a rate decrease. This may be due to the increase in temperature of the electrodes. As the temperature is increased, the etching process starts to take place. In order to overcome this problem, polymer deposition was stopped after 10 minutes, then let the substrate cool down under 1000 mTorr Ar pressure and start the deposition again. In general it was noticed that the polymer film has very high transmittance (Fig. A.9) about 100% which indicates a very clear, transparent, and weakly scattering amorphous film.

In this study gold, nickel and Si clusters embedded in a polymeric matrix were prepared by a capacitively coupled RF (13.56 MHz) sputtering system. TEM micrographs revealed that, changing the deposition time, gold clusters of size 30 to 500 Å were obtained, whereas, for nickel, clusters of size 20 to 100 Å were achieved. From Fig. 8.1 and Fig. A.3 (Appendix A) it is evident that the number density of the clusters decreases for increasing cluster volume fraction x , which is due to the agglomeration of small clusters into a larger one. It is seen from the micrograph 8.1 and 8.4 that the average size of the nickel clusters is smaller than the gold clusters. By comparing Fig. 8.4 ($x = 13\%$ nickel) and Fig. A.3 ($x = 15\%$ gold) it can be suggested that the main difference between gold and nickel lies in the different distribution of the average cluster size for the same volume fraction. Fig. A.4 (Appendix A) shows electron diffraction pattern of gold sample with closed bright circles which confirms gold in crystalline form. From Fig. A.8 it is

observed that diffraction lines for nickel are broader than for gold, which can be attributed to the smaller size of the nickel clusters. Hence smaller numbers of atomic layers are participating in the electronic diffraction process. For Si samples, due to the reason of very close atomic numbers of both Si and polymer (oxygen and carbon) matrix, no visible TEM micrographs could be achieved.

From optical transmittance measurement of various gold samples, it was found that, the spectra exhibited a marked absorption band in the visible region, the so-called dielectric anomaly characteristic of isolated metallic particles embedded in a dielectric [13]. This absorption can be attributed to plasma-resonance absorption of the particles. Plasma-resonance absorption of metal island films, consisting of small metal particles, results from the plasma oscillation of conduction band electrons. Some samples showed an additional small absorption peak from 350-380 nm which indicates the bound-electron resonance or interband transition in bulk gold. Since the clusters are relatively large and interband transition seems to occur at the same wavelength for different films, it is reasonable to assume that the clusters themselves have the bulk optical constants. From the transmittance spectra it is noticed that the overall transmission of the gold film is decreasing as the numbers of deposited layers are increased, without changing the absorption band characteristics significantly. It means that there are same number of similar clusters in each metallic layer.

By comparing the spectra from Figures. 8.5, 8.6 and 8.7, 8.8 it is observed that, gold films separated by 2 minute (min) polymer layers appear more lossy than those samples with 5 min polymer layers. The absorption peaks for a 2 min gold deposits shifted towards the longer wavelength. Although the reason is not clear it seems that the size of the clusters depend on the polymer thickness. It may happen that 2 min polymer is more permeable so that the metal clusters have enough mobility to come into contact with one another, coalesce and become larger.

Fig. 8.10 depicts wavelength dependent transmittance for five different samples of gold deposited at various times, which exhibits the characteristic shift of the absorption maxima to longer wavelength, due to the increase in gold volume fraction, which is qualitatively in good accord with the Maxwell-Garnett (M-G) theory [37]. The absorption maxima is found shifting very rapidly with deposition time which is different from the results reported by Norman *et al.* [3]. In their experiment, slow change in absorption peak with film thickness was found. The relationship was approximately linear over the thickness interval investigated which is in good accord with ours as shown in Fig. 8.9, whereas those by Yamaguchi [35] and Truong [32] exhibit a weaker thickness dependence of the absorption peak. The discrepancies are probably caused by slightly different conditions for cluster growth in various experiments.

Transmittance spectra of gold clusters (Fig. A.5) deposited on glass substrates by ultrahigh-vacuum was investigated by Norman *et al.* [3]. They compared experimental findings with theoretical results based on the M-G type effective-medium approach. It is found that our results have satisfactory agreement with their theoretical and experimental curves, including nature and shape of the curve, very small absorption peak near 370 nm, the decreased visible transmission, and higher infrared transmission. The only difference is that we have higher transmission with thicker samples than Norman's samples (his samples were much more thinner than our samples), which indicates that their samples are much more lossy than ours. This difference may be due to the different growth conditions for the clusters.

The transmittance spectra of nickel clusters were characterized by an UV absorption and a higher transmittance in the near infra-red region. The UV absorption peaks around 350-390 nm shown in Fig. A.1 and A.2 arise from plasma resonance i.e., a collective oscillation of the conduction electrons of the particles. Fig. 8.11 depicts that the shift in the absorption peak to the longer wavelength with deposition time is very small, which is substantially different from gold. This can be explained by the very slow growth

rate of cluster size. It is seen from Fig. 8.12 that the relationship between the wavelength of absorption maxima and deposition time is nonlinear which is different from gold. No interband transition was found for bulk nickel material.

The transmittance spectra in Figs A.10-A.12 for Si showed an absorption band in the UV region around 380 nm. This absorption band may arise from interband transition. Fig. A.10 shows the spectra of two Si samples prepared by two different sputtering system. They both reflect interband absorption which almost coincides. In Fig. A.12 for curve 1 (12 min Si) an absorption band in the region of 500-600 nm is observed whereas for 6 min Si (curve 2 and 3) it disappears. It can be concluded that this absorption peak is due to the particle size. In Fig. A.11 it is noticed that for curve 2, absorption peak has shifted to the longer wavelength compared to curve 1, which again confirms the cluster size effects.

The anomalous absorption peak found for gold, nickel and silicon was verified by reflection measurement. An attempt was made to verify whether these absorption peaks arise from the instrumental error or light scattering. It should be mentioned here that the size of the particles were orders of magnitude smaller than the wavelength of light used in this experiment. There was a very little chance to have a scattering effect from those particles. The typical behavior of the reflection R and transmission T, both at 45° incidence, for gold, nickel and silicon films are shown in Fig. 8.13 - 8.15. The samples were normalized to the reflectance of a polymer coated glass substrate and metal or silicon samples had higher reflectivity than polymer samples. Due to this reason the reflectance curves have more than 100% reflection. Near the region where the larger dip of T occurs, the curves for R display a rise, to a peak sometimes at a slightly smaller wavelength and sometimes at a slightly longer wavelength. Therefore, it can be suggested that the minimum in transmission for gold and nickel appeared truly from the plasma resonance absorption of the particles and for silicon it was from interband transition for bulk material.

Deposition of silicon was much more difficult than of gold or nickel. Thermal resistivity of Si is higher comparing with the metals. For this reason, after each 2 min deposition was stopped, let the target cool down in 1000 mTorr Ar for at least 5 min, then start deposition again. It is a time consuming process. To overcome this problem there should be cooling system which keeps the target cool. In this way thermal evaporation of the target material can also be prevented. The deposition rate of gold was $46 \text{ \AA}/\text{min}$ and for nickel it was $12 \text{ \AA}/\text{min}$. For silicon it was lower than nickel. In fact the rate of deposition in our system is lower than that of reported by other authors [7,17,36]. This difference can be expected to influence the cluster growth mechanism which in turn can effect the properties of the films.

CHAPTER 10

CONCLUSIONS

Sputtering of gold, nickel, and silicon and plasma polymerization of Methyl Methacrylate monomer resulted in the films consisting of an amorphous polymer matrix with embedded metal or silicon clusters. In this thesis a multilayered (metal or silicon/polymer) system was investigated. Metal clusters, sputtered at different deposition time, have been analyzed by both optical absorption and transmission electron microscopy (TEM) techniques. TEM analysis revealed that, depending on the deposition time and metal content, diameters of gold and nickel clusters vary from 30 to 500 Å and 20 to 100 Å, respectively. Furthermore, gold clusters were found to be much larger than nickel clusters at equivalent volume fractions. Electron diffraction patterns confirmed the crystallinity of gold and nickel clusters. The transmission characteristics, such as, the absorption maxima, width, and intensity of plasma absorption were found to be different upon varying the deposition time of metal or Si/polymer system.

An anomalous absorption band occurred for gold in the visible region (around 700 nm) whereas, for nickel it was in the UV region (~ 360 nm). The existence of these absorption bands were verified by reflection measurements. An increase in the metal cluster size and volume fractions were found to shift the absorption band to a longer wavelength. This result agrees qualitatively with Maxwell-Garnett theory.

For future work this study can be extended to the measurement of magnetic and electrical properties of the clusters and an investigation of optical nonlinearity.

APPENDIX A

FIGURES SHOWING EXPERIMENTAL RESULTS

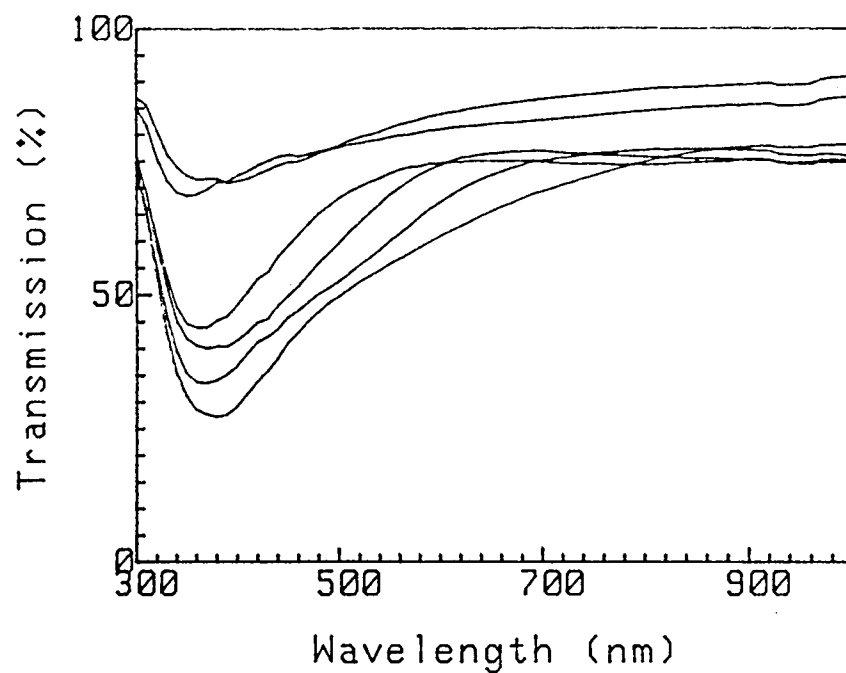


Figure A.1 Normal transmittance of successive nickel/polymer layers. Deposition time: Polymer 2 min, Nickel 10 min. Top curve-1st layer, Lowest curve-6th layer

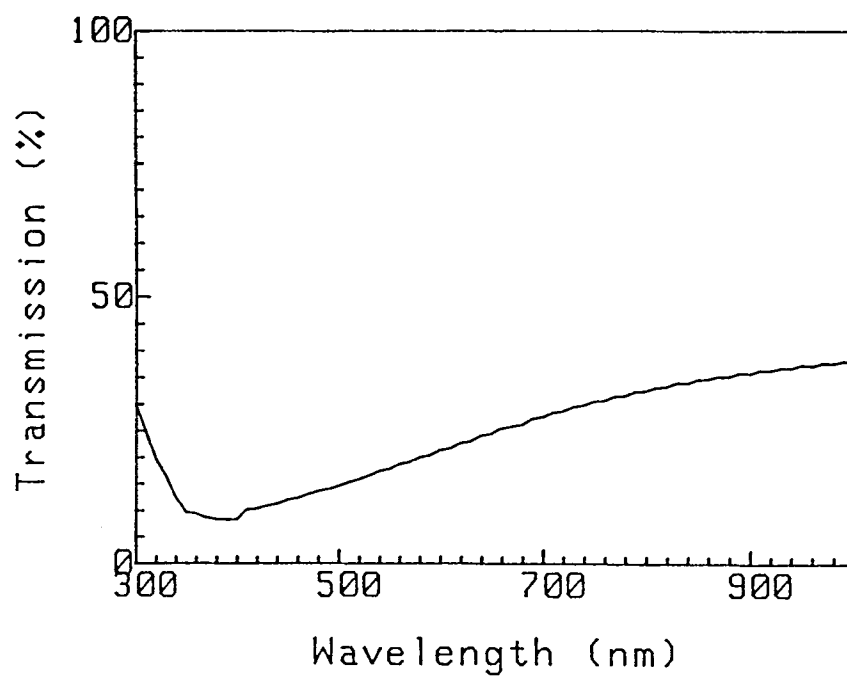
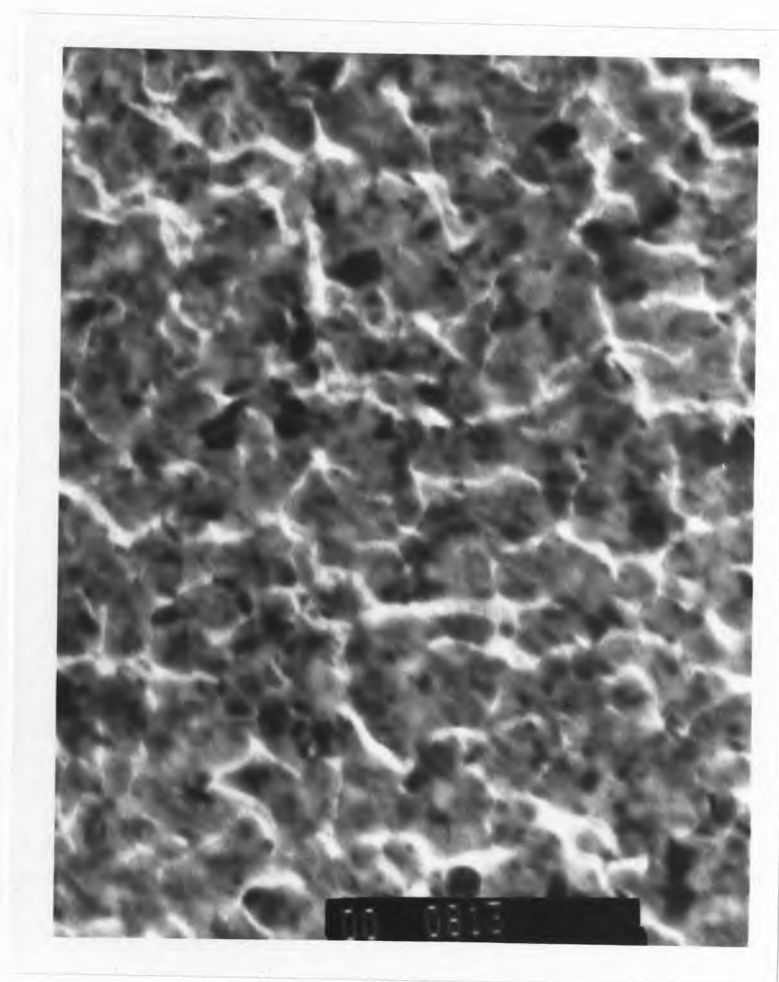


Figure A.2 Normal transmittance of three layers of nickel each 12 min separated by 5 min polymer



-----|
400 Å

Figure A.3 TEM micrographs of 45 sec deposited gold particles [$x = .15$]



Figure A.4 Electron diffraction pattern of 45 sec deposited gold. Closed bright circles represent crystallinity.

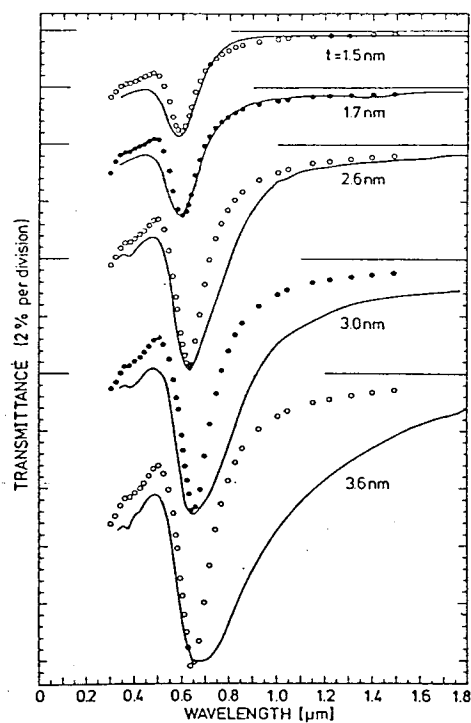


Figure A.5 Comparison of computed and measured optical transmittance (circles and solid curves) for discontinuous gold films with five mass thicknesses [3]

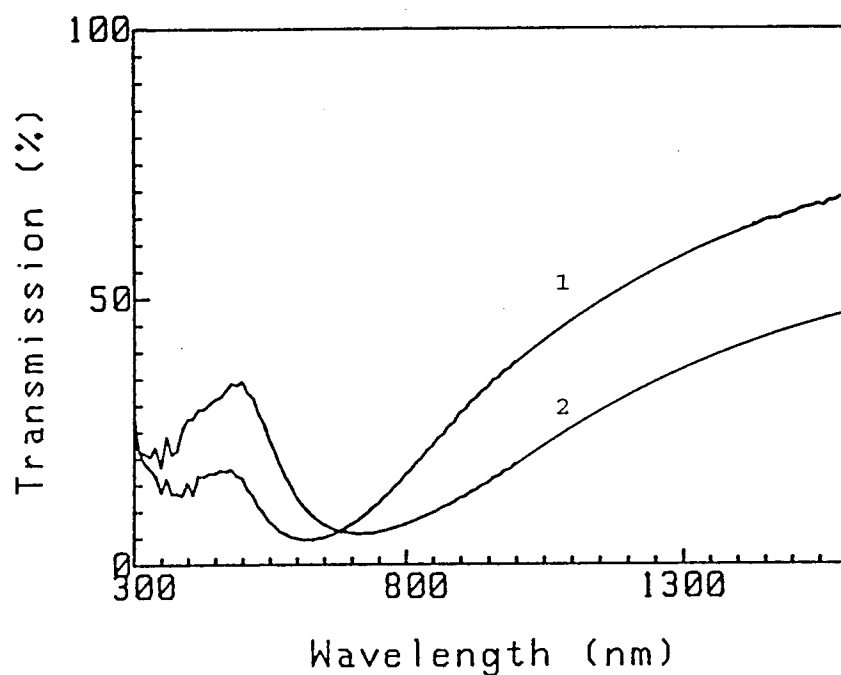
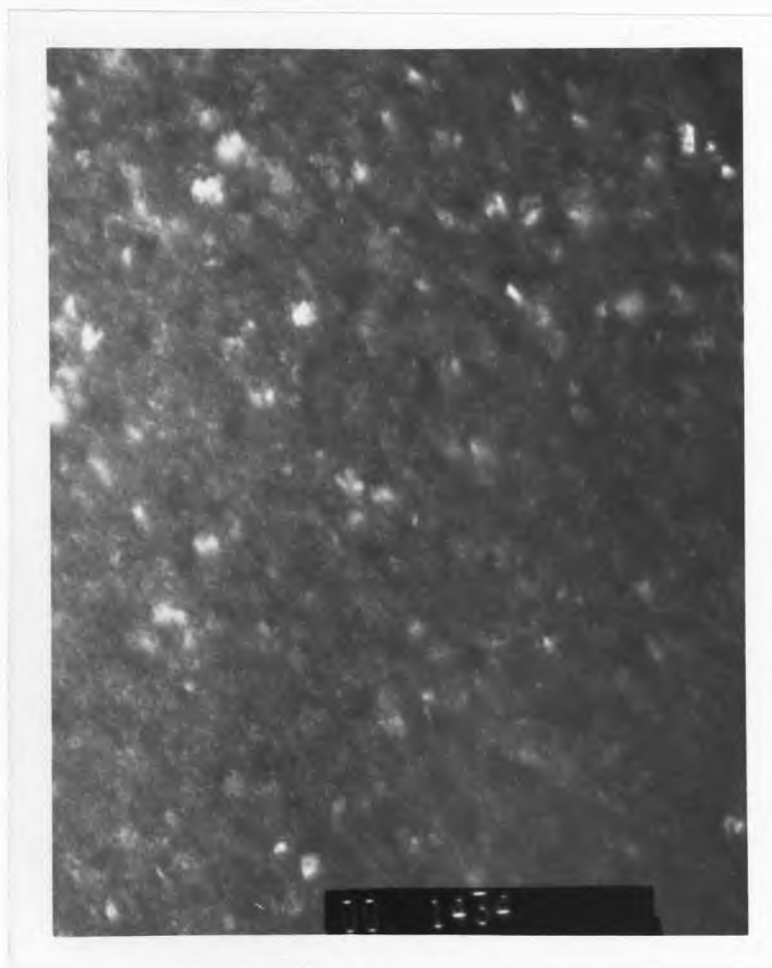


Figure A.6 Normal transmittance of six layers of gold for two different samples. (1) Deposition time: gold- 30 sec; polymer- 2 min. (2) gold- 1 min; polymer- 5 min



|-----|
300 Å

Figure A.7 TEM micrographs of 9 min deposited nickel particles [$x = .17$]

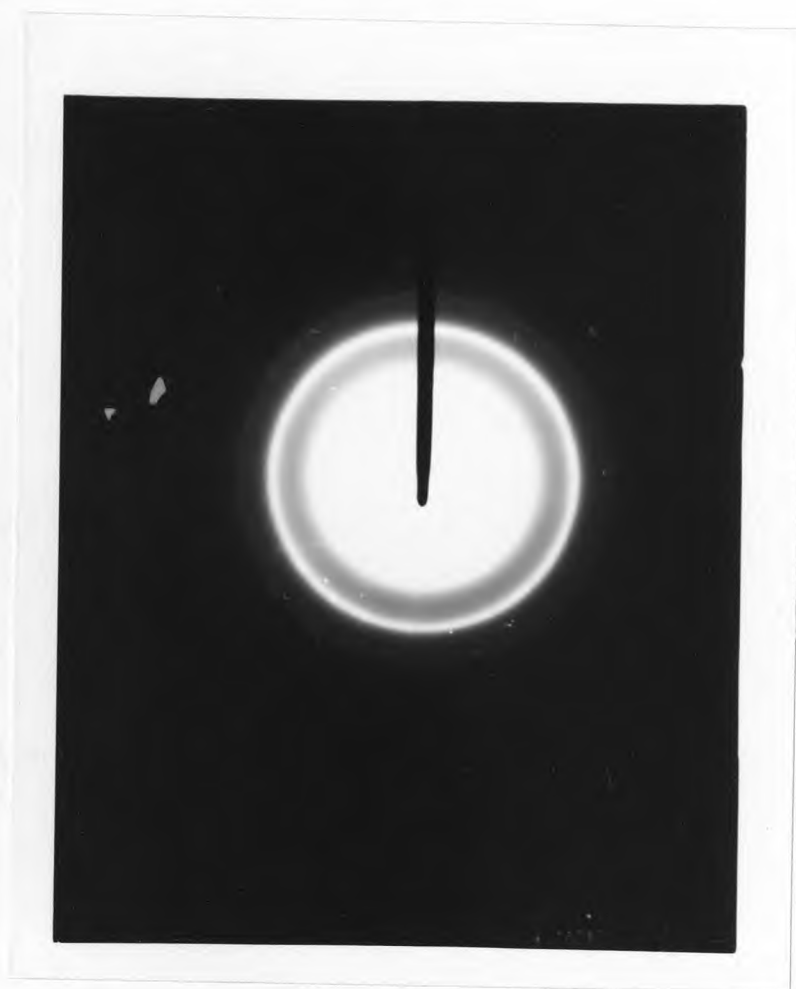


Figure A.8 Electron diffraction pattern of 9 min deposited nickel. Closed bright circles represent crystallinity.

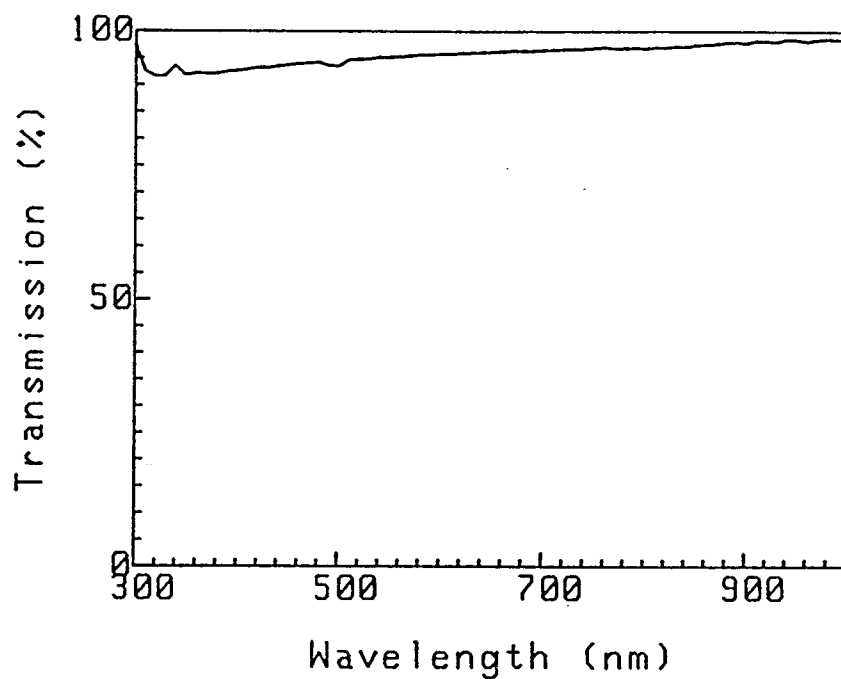


Figure A.9 Normal transmittance of 10 minute plasma polymerized methyl methacrylate

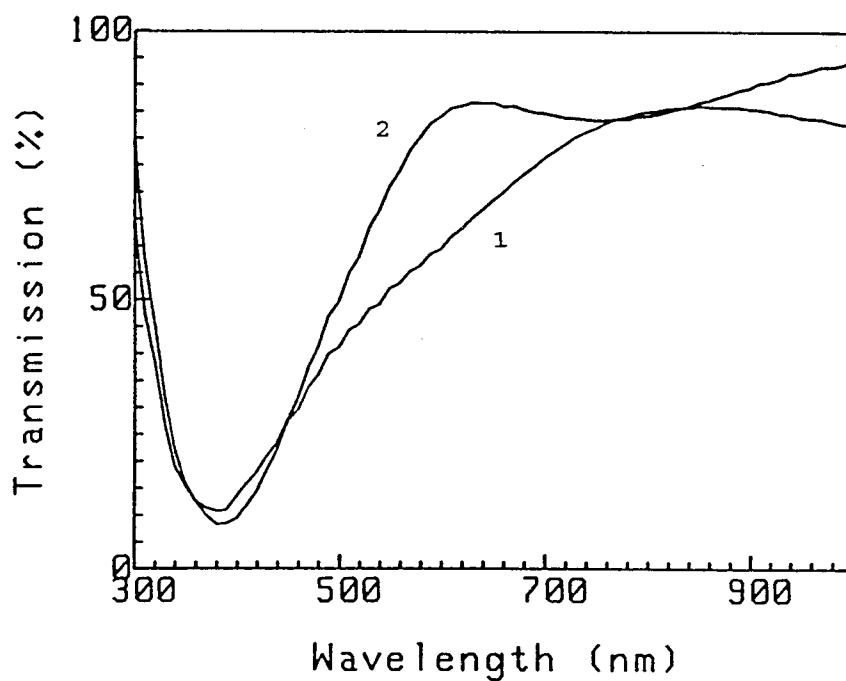


Figure A.10 Normal transmittance of one layer of silicon. (1) 30 min deposition by RF sputtering. (2) 30 min deposition by magnetron sputtering

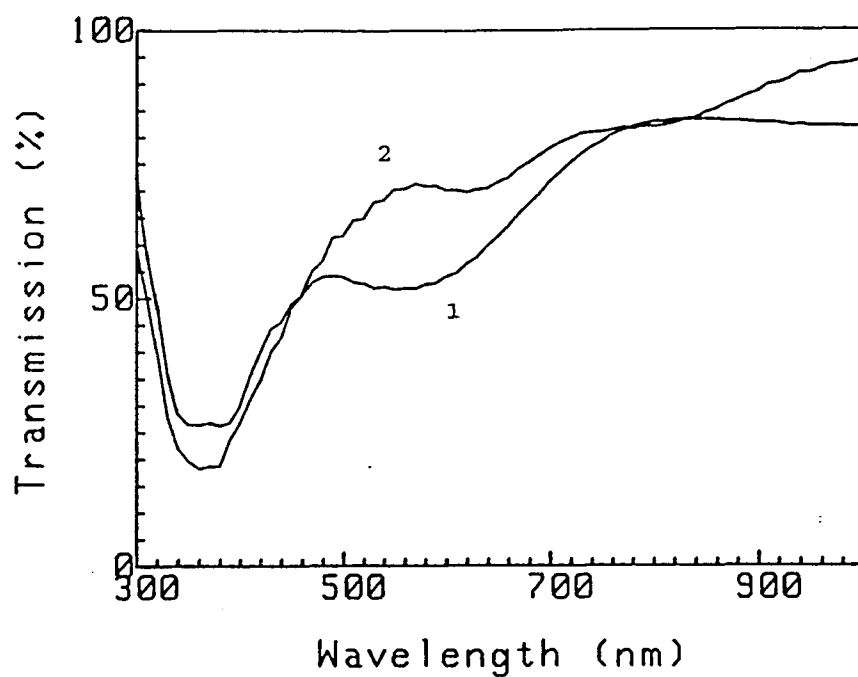


Figure A.11 Normal transmittance of successive silicon/polymer layers. (1) 3 layers of silicon (2) 6 layers of silicon. Deposition time: silicon-12 min; polymer-5 min

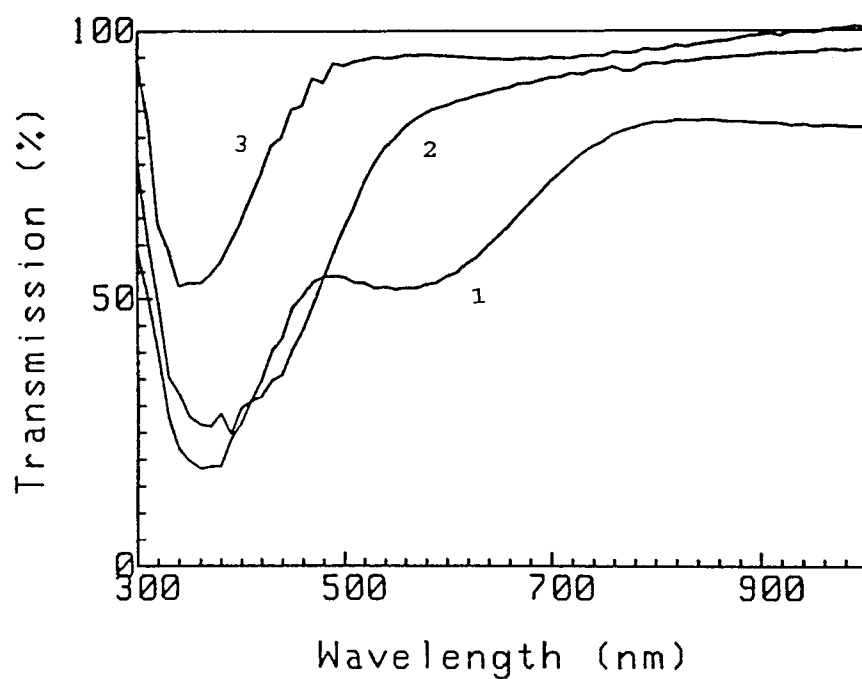


Figure A.12 Normal transmittance of successive silicon/polymer layers. (1) 3 layers of Si. Deposition time: Si-12 min; polymer-5 min (2) 4 layers of Si. Deposition time: Si-6 min; polymer-5 min. (3) 3 layers of Si. Deposition time: Si-6 min; polymer-5 min

APPENDIX B
COMPUTER PROGRAM FOR DATA COLLECTION

```

10  !SAMPLE PROGRAM TO CONTROL COMPUDRIVE AND LOCK-IN
    AMPLIFIER
20  ! USING HP300 COMPUTER
30  Dim A$[1], Data$[64], Space$[64]
40  Dim R$(410)[10]
50  Dim X(1:500), Y(1:500), W(1:500)
60  Dim A(1:500), B(1:500), P(1:500), Q(1:500)
70  Can$=CHR$(24)
80  Stx$=CHR$(2)
90  Etx$=CHR$(3)
100 Ack$=CHR$(6)
110 Nak$=CHR$(21)
120 Cd 4824=710 ! ADDRESS OF CD 4824
130 PRINTER IS CRT
140 Start: !
150 OUTPUT KBD USING " #, B, K" ; 255, "K" !CLEAR SCREEN
160 CLEAR SCREEN
170 PRINT " "
180 PRINT " "
190 PRINT " "
200 PRINT " "
210 PRINT "     OPTIONS: "
220 PRINT " "
230 PRINT "     1) OUTPUT COMMAND TO 4824 "
240 PRINT "     2) OUTPUT PARAMETER TO 4824 "
250 PRINT "     3) INITIALIZE 4824 "
260 PRINT "     4) EXIT TO BASIC "
270 PRINT " "
280 PRINT TABXY(1,20), "ENTER SELECTION:"
290 INPUT A$
300 SELECT A$[1]
310 CASE "1"
320     GOTO Outpt_c
330 CASE "2"
340     GOTO Outpt_p
350 CASE "3"
360     GOTO Init
370 CASE "4"
380     GOTO Fini
390 CASE ELSE
400     BEEP
410     GOTO Start
420 END SELECT
430 Outpt_c: !

```

```

440  !-----ABCD
450  GOTO 520
460  Data$=Space$ !CLEAR STRING DATA$
470  CLEAR SCREEN
480  PRINT TABXY(1,15), "S, T, H, E, P, OR X"
490  PRINT TABXY(1,20), "ENTER COMMAND TO OUTPUT TO 4824:"
500  INPUT Data$
510  IF Data$="X" THEN Data$=CHR$(14)
520  PRINT "ENTER THE INITIAL WAVELENGTH"
530  I=1
540  INPUT W(I)
550  IF W(I) < 290 OR W(I) > 1000 THEN
560  BEEP 81.38*8, 1
570  GOTO 520
580  END IF
590  PRINT "ENTER THE FINAL WAVELENGTH"
600  INPUT F
610  IF F < 290 OR F > 1000 THEN
620  BEEP 81.3*8, 1
630  GOTO 590
640  END IF
650  PRINT "ENTER INCREMENT OF WAVELENGTH"
660  INPUT M
670  IF M > 20 THEN
680  BEEP 81.3*8, 1
690  GOTO 650
700  END IF
710  N=(F-W(I))/M
720  FOR I=1 TO N+1 STEP 1
730  R$(I)=VAL$ (W(1) + (I-1) * M)
740  NEXT I
750  CLEAR SCREEN
760  PRINT "STARTING AT" ; W(1), "ENDING AT" ; F
770  PRINT
780  OUTPUT Cd4824; Stx$&Can$&Data$&Etx$ ! SEND STRING TO 4824
790  I=1
800  Set$="SE"
810  Data$=Set$&R$(I)
820  WAIT 1
830  ASSIGN @Path TO 710
840  OUTPUT Cd4824 ; Stx$&Data$&Etx$ ! SEND STRING TO 4824
850  Data$="P"
860  WAIT 1
870  OUTPUT Cd4824;Can$&Data$&Etx$
880  ENTER @Path; X(I)

```

```
890  OUTPUT @Path; Ack$
900  IF X(I)=W(I) THEN GOTO 920
910  GOTO 880
920  CALL Sensitiv
930  ASSIGN @Path TO 723
940  WAIT 3
950  G = 0
960  FOR J=1 TO 10
970  OUTPUT &Path; "Q"
980  WAIT .2
990  ENTER @Path; C
1000 G = G + C
1010 NEXT J
1020 Y(I) = G/10
1030 PRINT X(I), Y(I)
1040 IF W(I) = F THEN GOTO 1090
1050 I = I + 1
1060 W(I) = W(I - 1) + M
1070 ASSIGN @Path TO *
1080 GOTO 810
1090 BEEP
1100 Xmax = -1.0E + 308
1110 Ymax = -1.0E + 308
1120 Xmin = 1.0E + 308
1130 Ymin = 1.0E + 308
1140 FOR I = 1 TO N+1 STEP 1
1150 IF X(I) > Xmax THEN Xmax = X(I)
1160 IF X(I) < Xmin THEN Xmin = X(I)
1170 IF Y(I) > Ymax THEN Ymax = Y(I)
1180 IF Y(I) < Ymin THEN Ymin = Y(I)
1190 NEXT I
1200 PRINT "DO YOU WANT TO SAVE THE DATA(Y OR N) ?"
1210 INPUT A$
1220 IF A$="Y" THEN GOTO 1290
1230 IF A$="N" THEN GOTO 1250
1240 GOTO 1200
1250 INPUT "DO YOU WANT TO MEASURE AGAIN? (Y OR N)", F$
1260 IF F$="Y" THEN GOTO 520
1270 IF F$="N" THEN GOTO Start
1280 GOTO 1250
1290 PRINT "INPUT THE FILE NAME TO SAVE THE DATA"
1300 MASS STARGAGE IS " : , 700, 1"
1310 ENTER 2; File$
1320 ON ERROR GOTO 1410
1330 CREATE BDAT File$, 8, 300
```

```

1340 ASSIGN @Path_2 TO File$
1350 FOR I=2 TO N+1 STEP 1
1360 OUTPUT @Path_2; X(I), Y(I)
1370 NEXT I
1380 ASSIGN @Path_2 *
1390 MASS STORAGE IS " : , 700,0"
1400 GOTO 1250
1410 PRINT "DUPLICATE FILE NAME. INPUT FILE NAME AGAIN."
1420 GOTO 1310
1430 OUTPUT Cd4824; Str$ !UNLISTEN
1440 WAIT 10
1450 GOTO Start
1460 Outpt_p: !
1470 Data$=Space$ !CLEAR STRING DATA$
1480 CLEAR SCREEN
1490 PRINT TABXY(1,15), "ST, EN, BI, SR, DT, TY, SH, SL, SE, NS, SD,
    OR LL"
1500 PRINT TABXY(1,20), "ENTER PARAMETER TO OUTPUT TO 4824: "
1510 INPUT Temp$
1520 CLEAR SCREEN
1530 PRINT TABXY(1,20), "ENTER NEW VALUE OF PARAMETER
    "&Temp$&" : "
1540 INPUT Data$
1550 Data$=Temp$&Data$
1560 OUTPUT Cd4824; Stx$&Data$&Etx$ !SEND STRING TO 4824
1570 Str$="UNL"
1580 OUTPUT Cd4824; Str$ !UNLISTEN
1590 GOTO Start
1600 Init: !
1610 Data$=Space$ !CLEAR STRING DATA$
1620 CLEAR SCREEN
1630 PRINT TABXY(1,15), "INITIALIZE COMPUDRIVE 4824"
1640 PRINT " "
1650 PRINT " START POSITION = 290 "
1660 PRINT " END POSITION = 1000 "
1670 PRINT " SCAN TYPE = CONTINUOUS"
1680 PRINT " CONTINUOUS SCAN RATE = 10"
1690 PRINT " NUMBER OF SCANS = 1"
1700 Data$="ST290" ! START POSITION
1710 OUTPUT Cd4824; Stx$&Data$&Etx$ !SEND STRING TO 4824
1720 CALL Unlisten
1730 WAIT .3
1740 Data$="EN1000" ! END POSITION
1750 OUTPUT Cd4824; Stx$&Data$&Etx$ !SEND STRING TO 4824
1760 CALL Unlisten

```



```
1770 WAIT .3
1780 Data$="TYC" !SCAN TYPE
1790 OUTPUT Cd4824; Stx$&Data$&Etx$ !SEND STRING TO 4824
1800 CALL Unlisten
1810 WAIT .3
1820 Data$="SR10" !CONT SCAN TYPE
1830 OUTPUT Cd4824; Stx$&Data$&Etx$ !SEND STRING TO 4824
1840 CALL Unlisten
1850 WAIT .3
1860 OUTPUT Cd4824; Stx$&Data$&Etx$ !SEND STRING TO 4824
1870 CALL Unlisten
1880 PRINT " "
1890 PRINT "INITIALIZATION COMPLETE"
1900 BEEP
1910 WAIT 3
1920 GOTO Start
1930 Cler: !
1940 Str$="CLR"
1950 OUTPUT Cd4824; Str$ !CLEAR
1960 GOTO Start
1970 Fini: !
1980 STOP
1990 END
2000 SUB Unlisten
2010 Cd4824=710
2020 Str$="UNL"
2030 OUTPUT Cd4824; Str$ !UNLISTEN
2040 SUBEND
2050 SUB Sensitiv
2060 Pom=0
2070 CALL Otptq (Qn, Gn )
2080 CALL Range (An, Gn )
2090 IF ABS(Qn) > An THEN GOTO 2160
2100 IF Pom > 0 THEN GOTO 2200
2110 Pom=Pom+1
2120 Gn=Gn-1
2130 CALL Otptg(Gn)
2140 CALL Otptq(Qn, Gn)
2150 GOTO 2090
2160 Gn=Gn+1
2170 Pom=Pom+1
2180 CALL Otptg(Gn)
2190 GOTO 2070
2200 SUBEND
2210 SUB Otptg(Bb)
```

```
2220 ASSIGN @Path TO 723
2230 SELECT (Bb)
2240 CASE 1
2250 OUTPUT @Path; "G 10"
2260 GOTO 2960
2270 CASE 2
2280 OUTPUT @Path; "G 10"
2290 GOTO 2960
2300 CASE 3
2310 OUTPUT @Path; "G 10"
2320 GOTO 2960
2330 CASE 4
2340 OUTPUT @Path; "G 10"
2350 GOTO 2960
2360 CASE 5
2370 OUTPUT @Path; "G 10"
2380 GOTO 2960
2390 CASE 6
2400 OUTPUT @Path; "G 10"
2410 GOTO 2960
2420 CASE 7
2430 OUTPUT @Path; "G 10"
2440 GOTO 2960
2450 CASE 8
2460 OUTPUT @Path; "G 10"
2470 GOTO 2960
2480 CASE 9
2490 OUTPUT @Path; "G 10"
2500 GOTO 2960
2510 CASE 10
2520 OUTPUT @Path; "G 10"
2530 GOTO 2960
2540 CASE 11
2550 OUTPUT @Path; "G 11"
2560 GOTO 2960
2570 CASE 12
2580 OUTPUT @Path; "G 12"
2590 GOTO 2960
2600 CASE 13
2610 OUTPUT @Path; "G 13"
2620 GOTO 2960
2630 CASE 14
2640 OUTPUT @Path; "G 14"
2650 GOTO 2960
2660 CASE 15
```

```
2670 OUTPUT @Path; "G 15"
2680 GOTO 2960
2690 CASE 16
2700 OUTPUT @Path; "G 16"
2710 GOTO 2960
2720 CASE 17
2730 OUTPUT @Path; "G 17"
2740 GOTO 2960
2750 CASE 18
2760 OUTPUT @Path; "G 18"
2770 GOTO 2960
2780 CASE 19
2790 OUTPUT @Path; "G 19"
2800 GOTO 2960
2810 CASE 20
2820 OUTPUT @Path; "G 20"
2830 GOTO 2960
2840 CASE 21
2850 OUTPUT @Path; "G 21"
2860 GOTO 2960
2870 CASE 22
2880 OUTPUT @Path; "G 22"
2890 GOTO 2960
2900 CASE 23
2910 OUTPUT @Path; "G 23"
2920 GOTO 2960
2930 CASE 24
2940 OUTPUT @Path; "G 24"
2950 END SELECT
2960 WAIT 1
2970 SUBEND
2980 SUB Range(Aa, Bb)
2990 SELECT (Bb)
3000 CASE 1
3010 Aa=5.E-9
3020 GOTO 3720
3030 CASE 2
3040 Aa=1.E-8
3050 GOTO 3720
3060 CASE 3
3070 Aa=2.E-8
3080 GOTO 3720
3090 CASE 4
3100 Aa=5.E-8
3110 GOTO 3720
```

3120 CASE 5
3130 Aa=1.E-7
3140 GOTO 3720
3150 CASE 6
3160 Aa=2.E-7
3170 GOTO 3720
3180 CASE 7
3190 Aa=5.E-7
3200 GOTO 3720
3210 CASE 8
3220 Aa=1.E-6
3230 GOTO 3720
3240 CASE 9
3250 Aa=2.E-6
3260 GOTO 3720
3270 CASE 10
3280 Aa=5.E-6
3290 GOTO 3720
3300 CASE 11
3310 Aa=1.E-5
3320 GOTO 3720
3330 CASE 12
3340 Aa=2.E-5
3350 GOTO 3720
3360 CASE 13
3370 Aa=5.E-5
3380 GOTO 3720
3390 CASE 14
3400 Aa=1.E-4
3410 GOTO 3720
3420 CASE 15
3430 Aa=2.E-4
3440 GOTO 3720
3450 CASE 16
3460 Aa=5.E-4
3470 GOTO 3720
3480 CASE 17
3490 Aa=1.E-3
3500 GOTO 3720
3510 CASE 18
3520 Aa=2.E-3
3530 GOTO 3720
3540 CASE 19
3550 Aa=5.E-3
3560 GOTO 3720

```
3570 CASE 20
3580 Aa= .01
3590 GOTO 3720
3600 CASE 21
3610 Aa= .02
3620 GOTO 3720
3630 CASE 22
3640 Aa= .05
3650 GOTO 3720
3660 CASE 23
3670 Aa= .1
3680 GOTO 3720
3690 CASE 24
3700 Aa= .2
3710 END SELECT
3720 SUBEND
3730 SUB Otptq (Cc, Bb)
3740 ASSIGN @Path TO 723
3750 FOR I=1 TO 10
3760 ON TIMEOUT 7, 1 GOTO 3790
3770 ENTER @Path; Tym
3780 NEXT I
3790 Cc=0
3800 Bb=0
3810 OUTPUT @Path; "Q"
3820 ENTER @Path; Cc
3830 OUTPUT @Path; "G"
3840 ENTER @Path; Bb
3850 ASSIGN @Path TO *
3860 SUBEND
```

BIBLIOGRAPHY

1. Doremus, R. H. "Optical Properties of Thin Metallic Films in Island Form." *J. Appl. Phys.* 37 (1966): 2775-2782
2. Tokarsky, R. W., and J. P. Marton. "Optical Properties of Aggregated Ag and Au Thin Films-MG approach." *J. Appl. Phys.* 45 (1974): 3051-3058
3. Norman, S., T. Andersson, C. G. Granqvist, and O. Hunderi. "Optical Properties of Discontinuous Gold Films." *Phys. Rev. B* 18 (1978): 674-695
4. Grebel, H., and P.Chen. "Artificial Dielectric Polymeric Waveguides: Metallic Embedded Films." *J. Opt. Soc. Am. A.* 8 (1991): 615-619
5. Parmigiani, F., G. Samoggia, and G. P. Ferraris. "Optical Properties of Sputtered Gold Clusters." *J. Appl. Phys.* 57 (1985):2524-2528
6. Laurent, C., and E. Kay. "Properties of Metal Clusters in Plasma Polymerized Hydrocarbon Versus Fluorocarbon Matrices." *J. Appl. Phys.* 65 (1989): 1717-1723
7. Kay, E., A. Dilks, and U. Hetzler. "Incorporation of Metals into Fluoropolymer Films Synthesized by Plasma Technique." *J. Macromol. Sci. Chem. A.* 12 (1978): 1393-1398
8. Kay, E., and M. Hecq. "Metal Clusters in Plasma Polymerized Fluorocarbon Films: Cobalt-Aluminum." *J. Vac Sci. Technol. A.* 2 (1984): 401-404
9. Kay, E., and M. Hecq. "Metal Clusters in Plasma Polymerized Matrices: Gold." *Journal of Applied Physics.* 55 (1984): 370-374
10. Grebel, H. "Conditional Artificial Dielectrics." *Final Report for the New Jersey Commission on Science and Technology.* (1994): 5-6
11. Perrin, J., B. Despax, V. Hanchett, and E. Kay. "Microstructure and Electrical Conductivity of Plasma Deposited Gold/Fluorocarbon Composite Films." *J. Vac. Sci. Technol. A.* 4 (1986): 46-51
12. Laurent, C., E. Kay, and N. Souag. "Dielectric Breakdown of Polymer Films Containing Metal Clusters." *J. Appl. Phys.* 64 (1988): 336-343
13. Perrin, J., B. Despax, and E. Kay. "Optical Properties and Microstructure of Gold-Fluorocarbon-Polymer Composite Films." *Phys. Rev. B* 32 (1985): 719-731

BIBLIOGRAPHY
(Continued)

14. Martinnu, L., H. Biederman, and J. Nedbal. *Thin Solid Films* 136 (1986): 11
15. Biederman, H. "Metal Doped Polymer Films Prepared by Plasma Polymerization and Their Potential Applications." *Vacuum* 34 (1984): 405-410
16. Comita, P. B., W. Jacob, E. Kay, and R. Zhang. "Laser Coalescence of Gold Clusters in Gold-Fluorocarbon Composite Films." *SPIE Vol. 1804 Rapid Thermal and Laser Processing*. 1992: 154-160
17. Kunz, M. S., Kenneth R. Shull, and Andrew J. Kellock. "Morphologies of Discontinuous Gold Films on Amorphous Polymer Substrates." *J. Appl. Phys.* 72 (1992): 4458-4460
18. Eckertova, Ludmila. *Physics of Thin Films*. Plenum Press, A Div. of Plenum Publishing Corporation, New York, U. S. A. (1980)
19. Wolf, S., and R. N. Tauber. *Si Processing for the VLSI Era. Vol. 1, Process Technology*. Lattice Press, California, U. S. A. 1986
20. Maissel and Glang. *Handbook of Thin Film Technology*. Mcgraw-Hill Book Company, New York, 1983: 8-33
21. Taguchi, T., and A. Hiraki. "Preparation and Characterization of II-VI Semiconductor Films by sputtering." *Ion Beam Assisted Film Growth*. chapter 3, Edited by Tadatsugu Itoh. Elsevier Science Publishers, New York, 1989.
22. Bauer, S. H., and D. J. Frurip. "Homogeneous Nucleation in Metal Vapors. 5. A Self-Consistent Kinetic Model." *J. Phys. Chem.* 81 (1977): 1015-1024
23. Neidermayer, R. "Formation of Ad-layers and Clusters on Condensation of Metal Vapors on Solid Surfaces." *Angew. Chem. Int. Ed. Engl.* 14 (1975): 212-218
24. Weeks, J. D., and G. H. Gilmer. "Dynamics of Crystal Growth." *Adv. Chem. Phys.* 40 (1979): 157-228
25. Meeten, G. H. *Optical Properties of Polymers*. chapter 1, Elsevier Applied Science Publishers, England, 1986.
26. Kay, E., and A. Dilks. "Plasma Polymerization of Fluorocarbons in rf Capacitively Coupled Diode System." *J. Vac. Sc. Tech.* 18 (1981): 1- 11

BIBLIOGRAPHY
(Continued)

27. Buss, R. J. "Molecular Reactions at Plasma-Polymerized Film Surfaces." *J. Appl. Phys.* 59 (1986): 2977-2982
28. Klimovic, J., O. Ulmann and L. Martinu. "Low-Temperature Luminescence of Plasma-Polymerized Poly(N-vinylcarbazole) Films." *Vacuum* 39 (1989): 23-25
29. Yasuda, H. *Plasma Polymerization*. Chap. 6 Academic Press, New York, U. S. A. 1985.
30. Biederman, H. "Polymer Films Prepared By Plasma Polymerization and Their Potential Application." *Vacuum*. 37 (1987): 367-373
31. Anno, Eiji, and R. Hoshino. "Influence of Lattice Defects on the Width of Plasma Resonance Absorption of Silver Island Films." *J. Phys. Soc. Japan* 50 (1981): 1209-1216
32. Truong, V. V., and G. D. Scott. "Optical Properties of Aggregated Gold Films." *J. Opt. Soc. Am.* 66 (1976): 124 - 131
33. Anno, E., and T. Yamaguchi. "Optical Absorption of Ni and Pd Particles: Enhanced Correlation Interaction Between Conduction Electrons." *Surface Science*. 286 (1993): 168-175
34. Moskovits, M., and J. E. Hulse. "The Ultraviolet-visible Spectra of Diatomic, Triatomic, and Higher Nickel Clusters." *J. Chem. Phys.* 66 (1977): 3988 - 3994
35. Yamaguchi, S. "The Resonance Type Absorption of Very Thin Silver and Gold Films." *J. Phys. Soc. Japan*. 15 (1960): 1577-1588
36. Creasy, W. R., J. A. Zimmerman, W. Jacob, and E. Kay. "Pyrolysis and Laser Ablation of Plasma-Polymerized Fluorocarbon Films: Effects of Gold Particles." *J. Appl. Phys.* 72 (1992): 2462-2471
37. Doremus, R. H. "Optical Properties of Thin Metallic Films in Islands Form." *J. Appl. Phys.* 37 (1966): 2775-2781
38. Neiman, G. C., and K. J. Klabunde. "Clustering of Free Atoms and Particles." *Thin Films From Free Atoms and Particles*. Edited by K. J. Klabunde. Academic Press Inc. Florida, U.S.A. 1985.